Carderock Division
Naval Surface Warfare Center
Bethesda, Maryland 20817-5700

NSWCCD-50-TR--2000/008 February 2000

Hydromechanics Directorate
Research and Development Report

RESULTS OF EXPERIMENTS WITH A SEGMENTED MODEL TO INVESTIGATE THE DISTRIBUTION OF THE HYDRODYNAMIC FORCES AND MOMENTS ON A STREAMLINED BODY OF REVOLUTION AT AN ANGLE OF ATTACK OR WITH A PITCHING ANGULAR VELOCITY

by

Eric F. Van Randwijck

and

Jerome P. Feldman

NSWCCD-50-TR--2000/008 RESULTS OF EXPERIMENTS WITH A SEGMENTED MODEL TO INVESTIGATE THE DISTRIBUTION OF THE HYDRODYNAMIC FORCES AND MOMENTS ON A STREAMLINED BODY OF REVOLUTION AT AN ANGLE OF ATTACK OR WITH A PITCHING ANGULAR VELOCITY

Approved for public release;
distribution is unlimited.

REPORT DOCUMENTATION PAGE			
1. Agency use.	2. Report date: Feb. 2000	3. Report type: Directorate Dates covered: 1968	
4. Title: Results of Experiments with a Segmented Model to Investigate the Distribution of the Hydrodynamic Forces and Moments on a Streamlined Body of Revolution at an Angle of Attack or with a Pitching Angular Velocity			5. Funding:
6. Authors: Eric F. Van Randwijck and and Jerome P. Feldman			
7. Performing organization: Naval Surface Warfare Center, Carderock Division 9500 MacArthur Boulevard Bethesda, MD 20817-5700			8. Report number: NSWCCD-50-TR-2000/008
9. Sponsoring organization: Office of Naval Research 800 North Quincy Street (ONR 333) Arlington, VA 22217-5660			10. Sponsor number:
11. Supplementary notes:			
12. Distribution statement: Approved for public release; distribution is unlimited.			12b. Distribution code:
13. Abstract: The hydrodynamic forces and moments which are developed on unappended streamlined bodies of revolution at small and large angles of attack or with a pitching angular velocity were investigated by captive-model experiments and by theory. The captive-model experiments were performed with a segmented model of a Series 58 body in the deep water basin of the David Taylor Model Basin and on the rotating arm. Exact and simplified potential flow theories were used to compute the hydrodynamic force distribution on Series 58 bodies, and comparisons were made with the experiments. An empirical method was developed to predict the static and rotary stability derivatives for unappended bodies.			
14. Subject terms: Submarine, Hydrodynamics, Potential Flow Theory, Captive-Model. Experiments, Segmented Model			15. Pages: 40 16. Price code:
17. Report classification: Unclassified	18. Page classification: Unclassified	19. Abstract classification: Unclassified	20. Abstract distribution: Unclassified

THIS PAGE INTENTIONALLY LEFT BLANK.

CONTENTS

THIS PAGE INTENTIONALLY LEFT BLANK.

FIGURES

CONVERSIONS TO METRIC UNITS

1 foot = 0.3048 meter
1 pound = 4.448 Newtons
1 knot = 0.5144 meter per second

NOMENCLATURE

A right-hand orthogonal reference frame is fixed in the body with the origin at the reference point. The longitudinal axis x is directed toward the forward end of the body, the transverse axis y is directed toward the starboard, and the normal axis z is directed toward the keel. The associated components of hydrodynamic force and linear velocity along the x, y, and z axes are X, Y, and Z, respectively, and u, v, and w, respectively. The associated components of hydrodynamic moment and angular velocity about the x, y, and z axes are K, M, and N, respectively, and p, q, and r, respectively. Quantities are nondimensionalized by the appropriate products of one-half the mass density of water ½ρ, powers of the characteristic length (usually the overall length) of the body ℓ, and powers of the velocity of the origin of the body axes relative to the fluid U. The additional symbols used in this report are defined as follows:

Symbol	Definition
A	Cross-sectional area of the body of revolution at a longitudinal location ξ
A_z	Projected normal area of the body of revolution
$a_1, a_2, a_3, a_4, a_5, a_6$	Coefficients of the sixth degree polynomial describing the body
C_{DC}	Cross-flow drag coefficient based on the projected normal area of the body
d	Maximum diameter of the body of revolution
I_y	Moment of inertia in pitch
k_1	Longitudinal added mass of a spheroid
k_2	Normal added mass of a spheroid
k'	Pitching added moment of inertia of a spheroid
ℓ	Overall length of the body of revolution
M	Hydrodynamic pitching moment about y-axis
M_q	First order coefficient used in representing M as a function of q
M_w	First order coefficient used in representing M as a function of w
$M_{w\|w\|}$	Second order coefficient used in represented M as a function of w
M_1	Munk pitching moment
m	Mass of the body of revolution

m_l ..... Added mass of the body of revolution

q ..... Pitching angular velocity component about the y-axis relative to the fluid

R ..... Reynolds number

R_c ..... Local cross-flow Reynolds number

R_l ..... Radius of the body of revolution at a longitudinal location

U ..... Linear velocity of the origin of the body axes relative to the fluid

u ..... Component of linear velocity in the direction of the x-axis

w ..... Component of linear velocity in the direction of the z-axis

$X_{\dot{u}}$ ..... Longitudinal added mass of the body of revolution

Z ..... Hydrodynamic normal force along the z-axis

Z_q ..... First order coefficient used in representing Z as a function of q

Z_w ..... First order coefficient used in representing Z as a function of w

$Z_{\dot{w}}$ ..... Normal added mass of the body of revolution

$Z_{w|w|}$ ..... Second order coefficient used in representing Z as a function of w

α ..... Angle of attack

η ..... Lateral axis of coordinate system with origin at the bow of the body

μ ..... $dm_l/d\xi$

ν ..... Kinematic viscosity of water

ξ ..... Longitudinal axis of coordinate system with origin at bow of the body

ρ ..... Mass density of water

$( )'$ ..... Nondimensional form of ( )

ABSTRACT

The hydrodynamic forces and moments which are developed on unappended streamlined bodies of revolution at small and large angles of attack or with a pitching angular velocity were investigated by captive-model experiments. The captive-model experiments were performed with a segmented model of a Series 58 body in the deep water basin of the David Taylor Model Basin and on the rotating arm. Potential flow theories were used to compute the hydrodynamic force distribution on Series 58 bodies, and comparisons were made with the experiments.

ADMINISTRATIVE INFORMATION

The work was funded by the Naval Ship Systems Command RDT&E Program, General Hydromechanics Research Sub Project SR0090101, Task 0102.

INTRODUCTION

A research program was undertaken to investigate the distribution of the hydrodynamic forces and moments which act on a deeply submerged streamlined body of revolution in forward motion at various steady angles of attack and rotating with various pitching angular velocities. The results of the experiments were to be used to validate a method for estimating the hydrodynamic force and moment coefficients for bodies of revolution under these conditions.

The determination of the lift developed by a submerged body moving through a viscous fluid by theoretical means has been one of the fundamental problems in the field of hydrodynamics. There is a need to better understand the mechanism by which the viscous lift is developed. A segmented model permits the accurate measurement of the longitudinal distribution of the normal force along the submerged body.

This report provides a brief survey of the literature, describes the model used for the experiments, the test apparatus and procedures, and the reduction and presentation of the data. In addition, the report describes the theory used to calculate the force distribution, presents the experimental and theoretical results, and compares the results of the experiments and the theory. Finally, the values of the calculated stability derivatives for a number of Series 58 bodies are compared with experimental results. The results were originally published in February 1998 in a slightly different format.

SURVEY OF THE LITERATURE

Many studies have been undertaken to develop a better understanding of the normal forces and pitching moments that act on an unappended body of revolution in forward motion at an angle of attack or rotating with a pitching angular velocity. References 1 through 7 indicate that the distribution of forces along the forebody of a body with a large fineness ratio at a relatively small angle of attack can be calculated from potential flow theory. These references indicate that viscous effects predominate along the afterbody, and that measured forces are smaller than the forces calculated using potential flow theory. In viscous flow, the boundary layer over the stern portion of the body separates, and this causes a reduction in the force calculated using potential

flow theory. Furthermore, as the flow passes along the body, vortices are formed on the leeward side of the hull analogous to the development of vortices behind a circular cylinder normal to the direction of the flow.

Based on these phenomena, methods have been developed to predict the hydrodynamic forces and moments on slender bodies of revolution with blunt-based afterbodies. The method given in Reference 3 assumes that the force on the body is the sum of a linear potential flow contribution and a nonlinear viscous flow contribution. Other methods which can be applied to bodies of revolution without blunt-based afterbodies, assume that the forces on the forebody can be calculated using potential flow theory, but the forces on the remainder of the body can be calculated using the distribution of local cross-flow drag. For these method the portion of the body over which potential flow theory is applied is estimated from empirical curves derived from experimental pitching moment data.

GENERAL CONSIDERATIONS

As indicated previously, the objective of this investigation was to develop a fundamental understanding of how the hydrodynamic forces are developed on a submerged body of revolution at an angle of attack or rotating with a pitching angular velocity. To accomplish this objective, an existing 15-foot model of the Series 58 was segmented and instrumented to measure the normal forces on each segment, as well as the total forces and moments acting on the body. The first phase of the experiments was performed in the straightline basin using the Planar Motion Mechanism. These experiments were conducted at deep submergence over a range of angles of attack up to 90 degrees at zero pitching angular velocity. The second phase of the experiments was conducted on the rotating arm over a range of radii (nondimensional pitching angular velocities) at zero angle of attack.

Calculations were made based on potential flow theory to determine the force distribution for small angles of attack and small angular velocities. In addition, comparisons were made between the force distribution obtained from the experiments and from the theory. The force distribution at larger angles of attack was calculated using cross-flow drag theory. A value of the cross-flow drag coefficient was determined to account for the nonlinearities in the forces and moments at larger angles of attack. A semi-empirical methods was used to calculate the forces and moments for angles of attack of less than 18 degrees for seven Series 58 configurations.

DESCRIPTION OF THE MODEL

The experiments were performed with Series 58 Model 4621. The mathematical formulation of the geometry of the Series 58 bodies is given in Reference 8. A sixth degree polynomial describes the shape of the body, and the coefficients of the polynomial are determined by the prismatic coefficient, the position of the maximum section, the nose radius, the tail radius, and the fineness ratio. The sixth degree polynomial is as follows:

$$\eta'^2 = a_1\xi' + a_2\xi'^2 + a_3\xi'^3 + a_4\xi'^4 + a_5\xi'^5 + a_6\xi'^6$$

where $\xi' = \xi/\ell$ and $\eta' = R_1/d$. The cross sectional area of the body at a specific longitudinal location is

$$A = \pi R_1^{\,2} = \pi d^2 \eta'^2$$

and

$$dA/d\xi = (\pi d^2/\ell)(a_1 + 2a_2\xi' + 3a_3\xi'^2 + 4a_4\xi'^3 + 5a_5\xi'^4 + 6a_6\xi'^5)$$

The coefficients for the polynomial that describes Model 4621 are as follows:

Coefficients of the Polynomial	Model 4621
a_1	1.000000
a_2	1.137153
a_3	-10.774885
a_4	19.784286
a_5	-16.792534
a_6	5.645977

The offsets of the body of revolution, which were calculated using the sixth degree polynomial, are as follows:

ξ'	Model 4621 η'
0.00	0.0000
0.05	0.2272
0.10	0.3200
0.15	0.3847
0.20	0.4312
0.25	0.4637
0.30	0.4848
0.35	0.4964
0.40	0.5000
0.45	0.4967
0.50	0.4872
0.55	0.4721
0.60	0.4513
0.65	0.4247
0.70	0.3919
0.75	0.3518
0.80	0.3036
0.85	0.2458
0.90	0.1771
0.95	0.0957
1.00	0.0000

The geometric characteristics of Model 4621 are as follows:

Geometric Characteristics	Model 4621
Length, feet	15.0
Diameter, feet	2.044
Nose radius, feet	0.1392
Tail radius, feet	0.0
Wetted surface, square feet	70.55
Volume, cubic feet	29.53
Location of the center of buoyancy from the nose, feet	6.6840
Fineness ratio	7.339
Wetted surface coefficient	0.7324
Location of the center of buoyancy in model lengths	0.4456

where the fineness ratio is ℓ/d and the wetted surface coefficient is the wetted surface divided by the quantity $\pi d\ell$.

Model 4621 was made of fiberglass and was cut through transversely at nine locations to provide ten segments of varying length. Each segment was connected to a heavy beam positioned at the centerline of the model by means of a modular force gage which measured only the normal force on the segment. A schematic arrangement of the segments and their attachment to the beam is shown in Figure 1.

Model 4621 was supported by two struts spaced 6.2 feet apart. The reference point corresponding to the center of buoyancy was located midway between the centerline of the gimbals associated with the two struts. Modular force gages were connected rigidly between the struts and the beam to measure the total forces and moments on the model. The model and beam were constructed to allow a 90-degree rotation of the model about its longitudinal centerline to permit measurement at large angles of attack of the forces perpendicular to the struts.

TEST APPARATUS AND PROCEDURES

The experiments were performed on Towing Carriage 2 in the deep water portion of the David Taylor Model Basin and on the Rotating Arm Facility. The straightline tests were conducted at angles of attack up to 18 degrees using the Planar Motion Mechanism described in Reference 9, and at angles of attack up to 90 degrees using the Yaw Table. The Rotating Arm Facility is described in Reference 10. The rotating arm experiments were performed over a range of towing radii R_t. Since the nondimensional pitching angular velocity is defined as

$$q' = \frac{q\ell}{U}$$

and the steady tangential velocity of the model is $U = qR_t$,

$$q' = \frac{\ell}{R_t}$$

Hence, as the towing radius decreases, the nondimensional pitching angular velocity increases.

For the tests in the straightline basin, the gages in the model were arranged to measure the forces parallel to the axes of the towing struts. However, for the experiments performed on the Yaw Table and on the rotating arm, the gages were located to measure the forces perpendicular to the strut axes.

The straightline Planar Motion Mechanism experiments were performed at speeds of 2, 4, and 5 knots corresponding to Reynolds number based on the overall length of the model of 4.7, 9.4, and 11.7 million, respectively. The straightline Yaw Table experiments were performed at speeds of up to 2.5 knots corresponding to a Reynolds number based on overall length of 5.8 million or a Reynolds number based on maximum diameter of 0.8 million. The rotating arm experiments were performed at speeds of between 3 and 5 knots corresponding to Reynolds numbers based on overall length of 7.0 and 11.7 million.

The instrumentation was read before and after each test run, and the data was recorded. At standstill, measurements were made at each of the tilt table angles used during the straightline tests to determine the weight tare for each segment and for the total model. Standstill tests were also performed on the rotating arm at various roll angles to determine the mass and inertia tares.

The data that were recorded for Segment 6 at high angles of attack appear to be unreliable. Hence, they are not shown in the figures and tables.

REDUCTION AND PRESENTATION OF DATA

The data obtained from the straightline and rotating arm experiments have been reduced to nondimensional coefficients in accordance with Reference 11. The nomenclature is based on Reference 12. The data are presented in graphical form in Figures 2 through 9. Figures 2 and 3 show the forces on the forward six segments and aft four segments, respectively, for the straightline tests conducted at angles of attack up to 18 degrees. Figure 4 shows the corresponding total forces on the model. The forces on each segment at angles of attack up to 90 degrees are shown in Figure 5, and the corresponding total force is shown in Figure 6. Forces on each segment for the rotating arm experiments are shown in Figures 7 and 8 for the forward and aft segments, respectively. The corresponding total force is shown in Figure 9.

The distribution of the nondimensional normal force and pitching moment static derivatives Z_w'

and M_w', respectively, are given in Figure 10. The derivatives were determined from slopes of the curves of force or moment verses body angle. All derivatives with respect to angular quantities are given as "per radian."

The distributions of the cross-flow drag coefficient based on projected lateral area are shown in Figure 11 for angles of attack of ±90 degrees. The distributions of the nondimensional normal force and pitching moment rotary derivatives Z_q' and M_q', respectively, are shown in Figure 12.

DISCUSSION OF RESULTS

PREDICTION METHODS

Methods that use potential flow theory for calculating the distribution of the hydrodynamic forces and moments on a body of revolution are discussed in References 1 through 7. The method discussed in Reference 5 is designated as the "exact method," whereas the method outlined herein is designated as the "simplified method."

The "simplified method" assumes that for elongated bodies of revolution (with relatively large fineness ratios) that are translating vertically the flow is approximately two dimensional along most of the length. As the body translates at a small angle of attack, it experiences longitudinal and normal components of the velocity U as follows:

$$u = U \cos \alpha$$

$$w = U \sin \alpha.$$

According to References 1, 13, and 14, the combined longitudinal and normal velocities of the body produce a Munk pitching moment M_1 due to potential flow which is a function of the longitudinal and normal added masses as follows:

$$M_1 = (X_{\dot{u}} - Z_{\dot{w}})uw.$$

The longitudinal and normal added masses of a neutrally buoyant spheroid are as follows:

$$X_{\dot{u}} = -k_1 m$$

and

$$Z_{\dot{w}} = -k_2 m,$$

respectively, where k_1 and k_2 can be calculated using the expressions in References 13 and 14. Hence,

$$M_1 = (k_2 - k_1)muw.$$

For large fineness ratios, the value of k_1 approaches zero, the value of k_2 approaches 1, and M_1

is approximately

$$M_1 = muw.$$

According to Reference 13, the added mass m_1 of a neutrally buoyant two-dimensional circular cylinder is

$$m_1 = -\rho A \ell$$

where A is the cross-sectional area of the cylinder and ℓ is the length of the cylinder. Hence, the added mass of an element $d\xi$ of a body of revolution is approximately

$$dm_1 = -(k_2 - k_1)\rho A d\xi$$

where k_1 and k_2 are the added masses for a spheroid of the same fineness ratio of the body of revolution and A is the cross sectional area at a location ξ from the nose of the body.

The hydrodynamic force developed on the element $d\xi$ is

$$dZ = \frac{d}{d\xi}[\frac{d(m_1 w)}{dt}]d\xi$$

or

$$dZ = uw\frac{d}{d\xi}[\frac{dm_1}{d\xi}]d\xi$$

Let

$$\mu = \frac{dm_1}{d\xi}$$

Then the normal force and pitching moment are

$$Z = uw \int d\mu$$

$$M = -uw \int x \, d\mu$$

Integrating the expression for normal force from the nose $\xi = 0$ to a longitudinal location $\xi = \xi_1$ gives

$$Z = -uw\,(k_2 - k_1)\rho A_1$$

where A_1 is the cross-sectional area at the longitudinal location $\xi = \xi_1$.

For the body rotating with a pitching angular velocity q, the normal force and pitching moment are

$$Z = -uq \int d(\mu x)$$

$$M = uq \int x\, d(\mu x)$$

where it is assumed that

$$\mu = -k'\rho A$$

where the added moment of inertia of a neutrally buoyancy spheroid is

$$M_{\dot{q}} = -k'I_y.$$

This expression is analogous to using the expression for the added mass $Z_{\dot{w}} - X_{\dot{u}} = -(k_2 - k_1)m$ for the case of a body translating with an angle of attack.

FORCE DISTRIBUTION AT SMALL AND MODERATE ANGLES OF ATTACK

The experimental force distribution on a submerged body of revolution provides information on the potential and viscous flow around the body. The results of the captive-model experiments are compared with calculations using the analytical methods.

Experimental Data

The results of the experiments at low to moderate angles of attack are shown in Figures 2 and 3 where the normal force coefficient is plotted as a function of angle of attack. As can be seen, for the forward section of the body (Segments 1 through 4) the force is essentially linear with angle of attack. This indicates that the flow is primarily potential. Segments aft of the point of maximum cross section of the body exhibit an increasingly nonlinear variation of the force with angle of attack which indicates that vortices are forming and possibly shedding from the body. Hence, with increasing distance along the afterbody, there is increasing viscous flow.

In Figure 4, the total normal force and pitching moment coefficients are given as a function of the angle of attack. As can be seen, the agreement between the total measured values and the sum of the individual values is satisfactory.

In Figure 13, the cross-flow drag coefficients for positive and negative angles of attack of 10 and 14 degrees are shown for each segment. As can be seen, there is a gradual increase in the cross-flow drag coefficient from about zero at the forward portion of the body to a maximum of about 1.4 at Segment 8 followed by a slight decrease at Segment 9. However, it is not possible to draw conclusions about the distribution of the cross-flow drag coefficient along the length of the body due to the complex three dimensional flow. It is likely that not only the Reynolds number based

on the cross-flow, but also the streamwise Reynolds number will influence the boundary layer.

Calculations

Calculations were performed using the "exact method." for Series Model 4157 rather than Model 4621 since the potential flow pressure and velocity distributions were available for Model 4157 rather than Model 4621. The geometric characteristics of Model 4157 are as follows:

Coefficient of Polynomial	Model 4157
a_1	1.000000
a_2	2.149653
a_3	-17.773496
a_4	36.716580
a_5	-33.511285
a_6	11.418548

Geometric Characteristics	Model 4157
Length, feet	9.0
Diameter, feet	1.286
Nose radius, feet	0.0918
Tail radius, feet	0.0184
Wetted surface, square feet	28.15
Volume, cubic feet	7.595
Location of the center of buoyancy from the nose, feet	4.180
Fineness ratio	7.000
Wetted surface coefficient	0.7744
Location of the center of buoyancy in model lengths	0.4644

The fineness ratios of Models 4621 and 4157 are 7.33 and 7.00, respectively. Hence, the force distribution computed for Model 4157 should approximate closely the distribution for Model 4621.

Comparison Between Analytical Methods

Figure 14 shows the cumulative values of the normal force and pitching moment derivatives as a function of distance from the nose for both the "exact method" and the "simplified method." It should be emphasized that the ordinate in Figure 14 for a particular distance from the nose ξ should be interpreted as the force or moment derivative for the blunt based body of length ξ with a cross sectional area A at the base. Hence the derivatives for the complete body are determined from the ordinate at the tail of the body. Based on potential flow theory, the normal force derivative for the complete body is zero, but the pitching moment derivative is equal to the Munk moment.

As can be seen in Figure 14, the agreement between the "exact method" and the "simplified method" is excellent for the moment derivative. However, the two methods predict different results for the force derivative near the midbody. As can be seen in Figures 15, 16, and 17, these trends are also applicable to Models 4156, 4158, and 4159, respectively, as well.

Comparison Between Analytical Methods and Experiments

Figure 10 shows a comparison between the experiments and the "simplified method" for the distribution of the force and moment derivatives for Model 4621. As can be seen, there is satisfactory agreement for Segments 1 through 7. However, for Segments 8 through 10, there is a discrepancy which is probably due to the increasing viscous flow at the stern.

An explanation for the discrepancy is that the fluid particles near the afterbody do not have sufficient kinetic energy to overcome the adverse pressure gradient along the suction side of the body. Hence, a reversal of the flow occurs, and a pair of rolled up trailing vortices is developed which at larger angles of attack is detached from the body to form a vortex sheet. The loss of kinetic energy in the boundary layer also results in an increase in pressure over the afterbody which causes an increase in lift on the body and a decrease in pitching moment. This can be seen in Figure 10 where the pitching moment derivatives at the stern are smaller than the values calculated from potential flow theory.

The cumulative values of the normal force and pitching moment derivatives are shown in Figure 18. The experimental data for Model 4621 are compared with calculations using the "exact method" and the "simplified method" for Model 4157. As can be seen, the experimental data are in better agreement with the "exact method" than with the "simplified method." Again, the agreement is excellent over the forebody, but poor over the afterbody. Consequently, it appears that the analytical methods are adequate for predicting the forces over about 80 percent of the body. Hence, the linear part of the normal force and pitching moment on a body of revolution can be determined by employing potential flow theory for the forces on the forebody and empirical methods for the forces on the afterbody. It is interesting to note that for blunt based bodies without an afterbody the hydrodynamic forces and moments can be calculated entirely from potential theory with excellent results.

FORCE DISTRIBUTION AT LARGE ANGLES OF ATTACK

The effect of large angles of attack on the normal force for each segment is shown in Figure 5. The fairing of the curves for the small angles of attack follows that shown in Figures 2 and 3. The data exhibits some scatter at 60 and 75 degrees due to unstable flow, and it is slightly different at positive and negative angles due to model asymmetries.

The data at an angle of attack of 90 degrees was converted to cross-flow drag coefficients C_{DC} as follows:

$$C_{DC} = (\ell^2/A_z)(Z')_{\alpha=90}$$

where A_z is the projected area of the body.

Figure 11 shows the cross-flow drag coefficients for each segment. Although the data were taken at various Reynolds numbers, there is no clear effect of Reynolds number except possibly for Segment 10. In addition, the cross-flow drag coefficient for the entire body is constant with Reynolds number for the range of Reynolds numbers at which the experiments were performed (0.48 to 0.80 million based on the diameter of the segment).

As shown in Figure 11, the cross-flow drag coefficients for the entire body at angles of attack of 90 degrees and -90 degrees are 0.61 and 0.59, respectively. It is interesting to note that the values of the cross-flow drag coefficient for Segments 3 through 9 are approximately between 0.55 and 0.60.

For angles of attack other than 90 degrees, a local cross-flow Reynolds number R_c was calculated as follows:

$$R_c = (U \sin \alpha)d/\nu$$

Reference 6 describes a technique for determining the cross-flow drag coefficient from normal force data for bodies of revolution at small and moderate angles of attack. The data was fitted to the following equation using the method of least squares to determine the values of the coefficients C_0, C_1, and C_2

$$Z' = C_0 \cos \alpha \cos \alpha + C_1 \sin \alpha \cos \alpha + C_2 \sin \alpha |\sin \alpha|$$

At an angle of attack of 90 degrees, $Z' = C_2$. Hence, the cross-flow drag coefficient C_{DC} was determined from the following equation:

$$C_{DC} = C_2 \ell^2/A_z$$

The values of the cross-flow drag coefficient at angles of attack of ±10 and ±14 degrees are shown in Figure 13. As can be seen, the cross-flow drag coefficients at these angles of attack varies over the afterbody from a value of about 0.2 at Segment 5 to a value of about 1.3 at Segment 8.

The values of the cross-flow drag coefficient at angles of attack of ±45, ±60, ±75, and ±90 degrees are shown in Figure 19 for Segments 1, 5, 7, and 8, as well as for the entire body as a function of the local cross-flow Reynolds number. The effect of angle of attack on the cross-flow drag coefficient is particularly large for Segment 1, but relatively small for the entire body.

FORCE DISTRIBUTION WITH SMALL PITCHING ANGULAR VELOCITIES

The force distribution on a body of revolution moving with small pitching or yawing angular velocities is discussed on the basis of the experiments performed on the rotating arm, potential flow theory, and a comparison between the theory and the experiments.

Experimental Data

Figures 7 and 8 show the normal force coefficient as a function of the nondimensional pitching angular velocity for the forward and aft segments, respectively. Figure 9 shows the same information for the entire model. The curves were faired as straight lines through the data points for the smaller angular velocities. As can be seen, Segments 1, 4, 5, and 6 exhibit almost entirely straight lines over the range of angular velocities evaluated, whereas segments 2, 7, 8, 9, and 10 exhibit nonlinearities even at small angular velocities.

Figure 9 shows the forces and moments for the entire model. The total forces and moments include a relatively small hydrodynamic contribution and a relatively large centrifugal force contribution. The scatter in the data is caused primarily by the difficulty of measuring accurately the relatively small hydrodynamic contribution.

The derivatives for each segment evaluated at zero angular velocity are shown in Figure 12. Cumulative values of the force and moment derivatives as a function of distance from the nose are shown in Figure 20. As can be seen, the derivatives for the entire body which are determined from the values of the ordinates at the tail of the body indicate that the force and moment derivatives with angular velocity are non-zero.

Calculations

The "exact method" was used to calculate the force distributions for several Series 58 bodies rotating with a pitching angular velocity. Figure 21 shows the force distribution for Model 4157. Figures 15, 16, and 17 show the force distribution for Models 4156, 4158, and 4159, respectively.

The "simplified method" was used to calculate the force distributions for Models 4157, 4156, 4158, and 4159, and these are shown in Figures 21, 15, 16, and 17, respectively. The distribution for Model 4621 is shown in Figures 12 and 20.

Comparison Between Analytical Methods

From Figures 15, 16, 17, and 21 it can be seen that the "simplified method" gives a good approximation of the exact distribution over a range of fineness ratios. The satisfactory agreement between the "exact method" and "simplified method" appears to validate the rather arbitrary

introduction of the added mass factors in the simplified technique for the calculation of the force distribution.

Comparison Between Analytical Methods and Experiments

Figure 12 shows a comparison between the "simplified method" and the experimental data for the distribution of the normal force and pitching moment derivatives with pitching angular velocity. As can be seen, the agreement is satisfactory except at the tail where viscous effects and flow separation become more significant. Figure 20 shows that the cumulative experimental force and moment derivatives agree with the analytical values except for Segment 10. Hence, it can be concluded that the "simplified method" when adjusted with the appropriate added mass factors gives a satisfactory representation of the actual force distribution along approximately 90 percent of the body of revolution rotating with a small angular velocity.

CONCLUSIONS

Based on the results of a program of captive-model experiments performed with a segmented model, analyses, and a comparison between the results of the experiments and the analyses, the following conclusions are drawn concerning the distribution of the hydrodynamic forces and moments on an unappended body of revolution.

1. The hydrodynamic force distribution at small angles of attack can be predicted satisfactorily by potential flow theory over about 80 percent of the length of the body. The remaining portion of the afterbody increasingly deviates from potential flow due to viscous effects.

2. At larger angles of attack, cross-flow drag develops on the afterbody which is dependent on the local cross-flow Reynolds number, the angle of attack, and the longitudinal location on the body.

3. At angles of attack of 90 degrees and -90 degrees, the cross-flow drag coefficient is found to be 0.61 and 0.59, respectively. The cross-flow drag coefficients for Segments 3 through 9 are between 0.55 and 0.60.

4. The hydrodynamic force distribution for angular velocity can be predicted satisfactorily by potential flow theory over about 90 percent of the length of the body.

REFERENCES

1. Munk, M.M., "The Aerodynamic Forces on Airship Hulls," NACA Report 184 (1923).

2. Durand, W. F., "Aerodynamic Theory," Volume VI (January 1943).

3. Allen, J. and E. Perkins, "A Study of Effects of Viscosity on Flow over Slender Inclined Bodies of Revolution," NACA Report 1048 (1951).

4. Sacks, A., "Aerodynamic Forces, Moments, and Stability Derivatives for Slender Bodies of General Cross Section," NACA Technical Note 3283 (November 1954).

5. Landweber, L., "Potential Flow About Bodies of Revolution and Symmetric Two-Dimensional Forms," Iowa Institute of Hydraulic Research, Iowa City, Iowa Report (December 1959).

6. Thwaites, B., "Incompressible Aerodynamics," Oxford University Press (1960).

7. Robinson, James M., "Hydrodynamics in Theory and Application," Prentice-Hall, Inc. (1965).

8. Landweber, L. and M. Gertler, "Mathematical Formulation of Bodies of Revolution," DTMB Report 719 (September 1950).

9. Gertler, M., "The DTMB Planar-Motion-Mechanism System," Naval Ship Research and Development Center Report 2523 (July 1967).

10. Brownell, W.F., "A Rotating Arm and Maneuvering Basin," DTMB Report 1053 (July 1956).

11. Goodman, A., "Experimental Techniques and Methods of Analysis Used in Submerged Body Research," Proceedings of the Third Symposium on Naval Hydrodynamics, Office of Naval Research (1960).

12. Imlay, F.H., "A Nomenclature for Stability and Control," David Taylor Model Basin Report 1319 (May 1959).

13. Lamb, H., "Hydrodynamics," Sixth Edition, Dover Publications, New York (1945).

14. Imlay, F.H., "The Complete Expressions for "Added Mass" of a Rigid Body Moving in an Ideal Fluid," David Taylor Model Basin Report 1528 (July 1961).

THIS PAGE INTENTIONALLY LEFT BLANK.

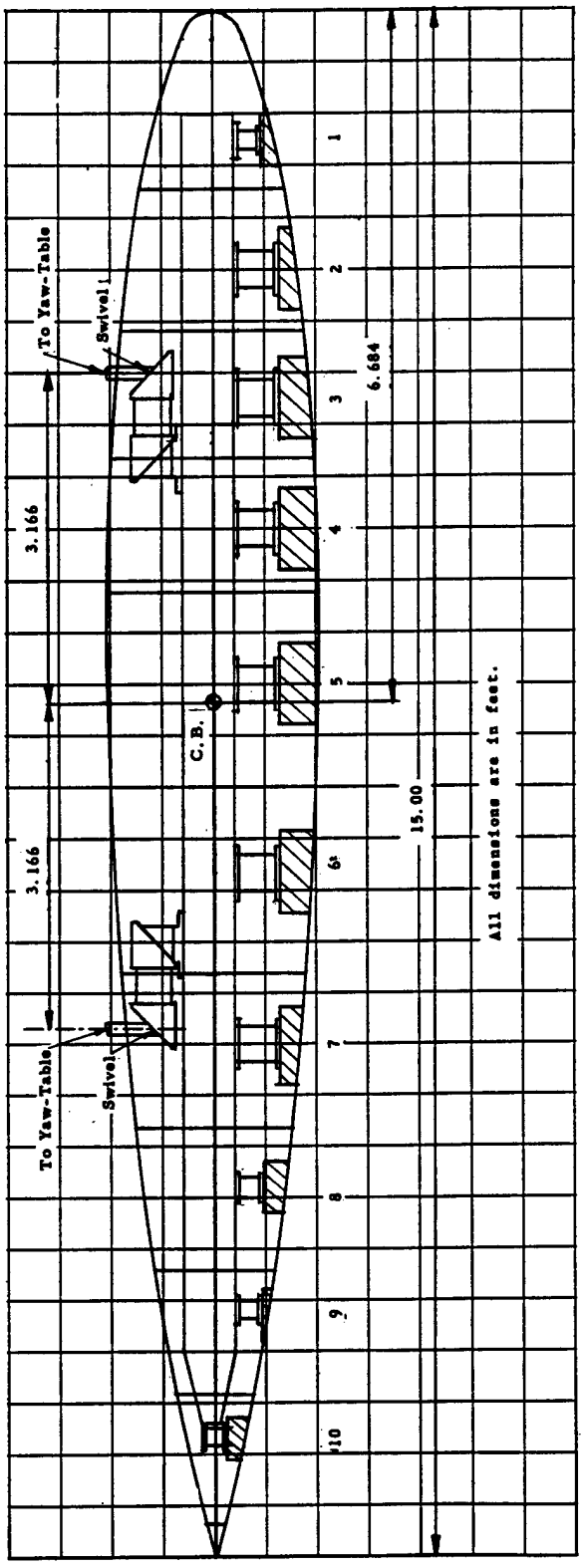

Fig. 1. Schematic sketch of the towing arrangement and force measuring apparatus.

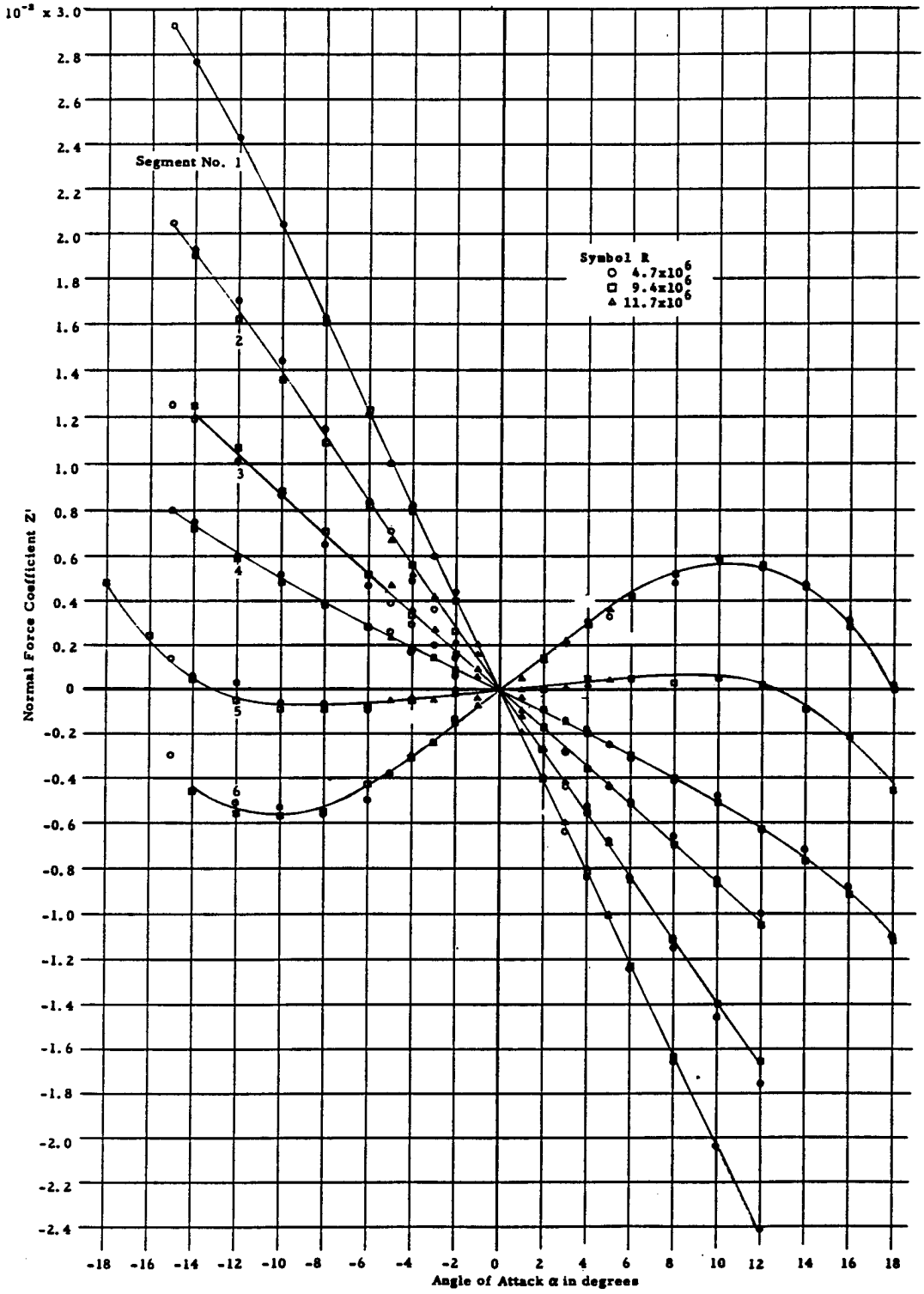

Fig. 2. Effect of angle of attack on the normal force coefficient for Segments 1 through 6.

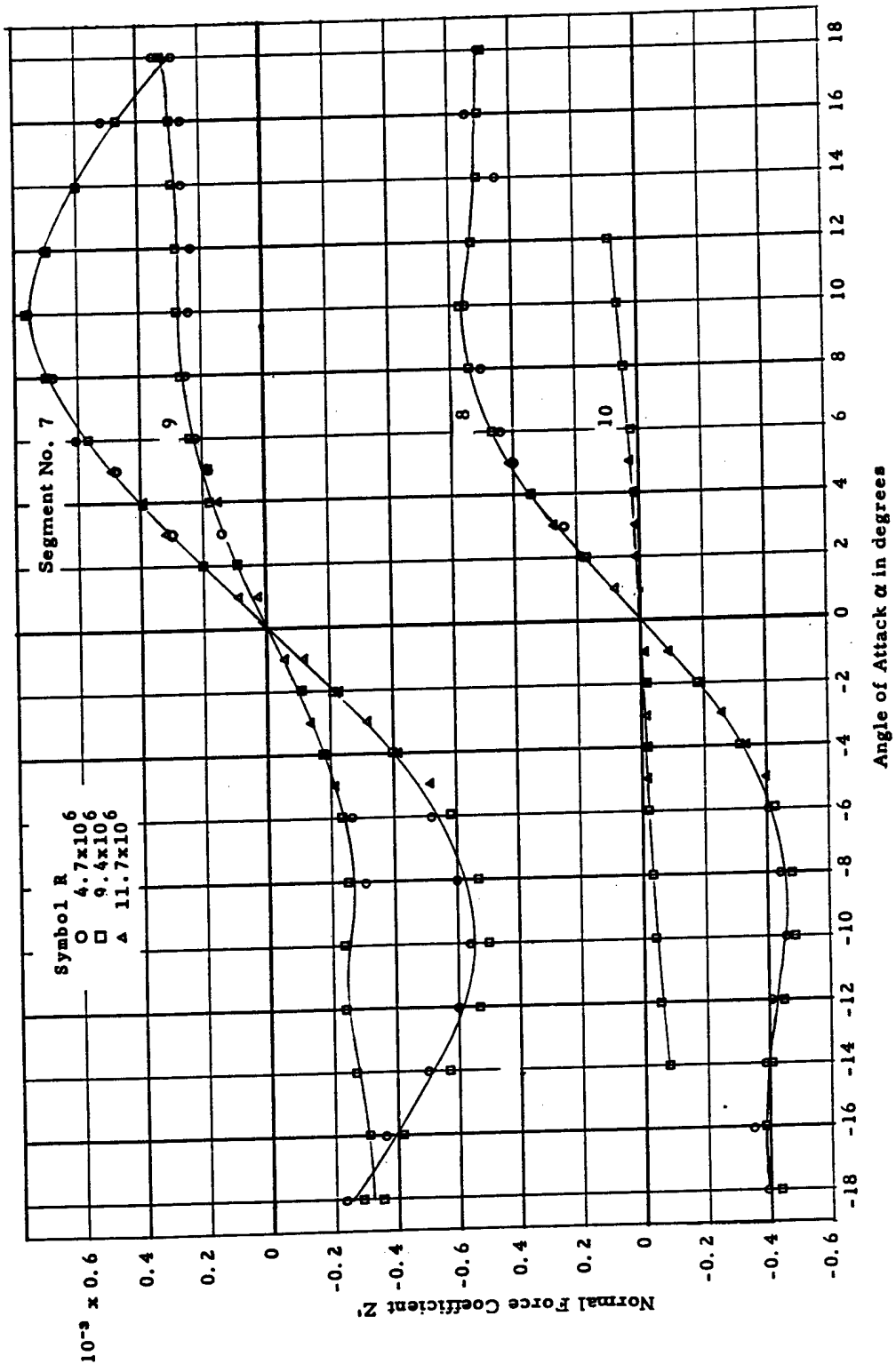

Fig. 3. Effect of angle of attack on the normal force coefficient for Segments 7 through 10

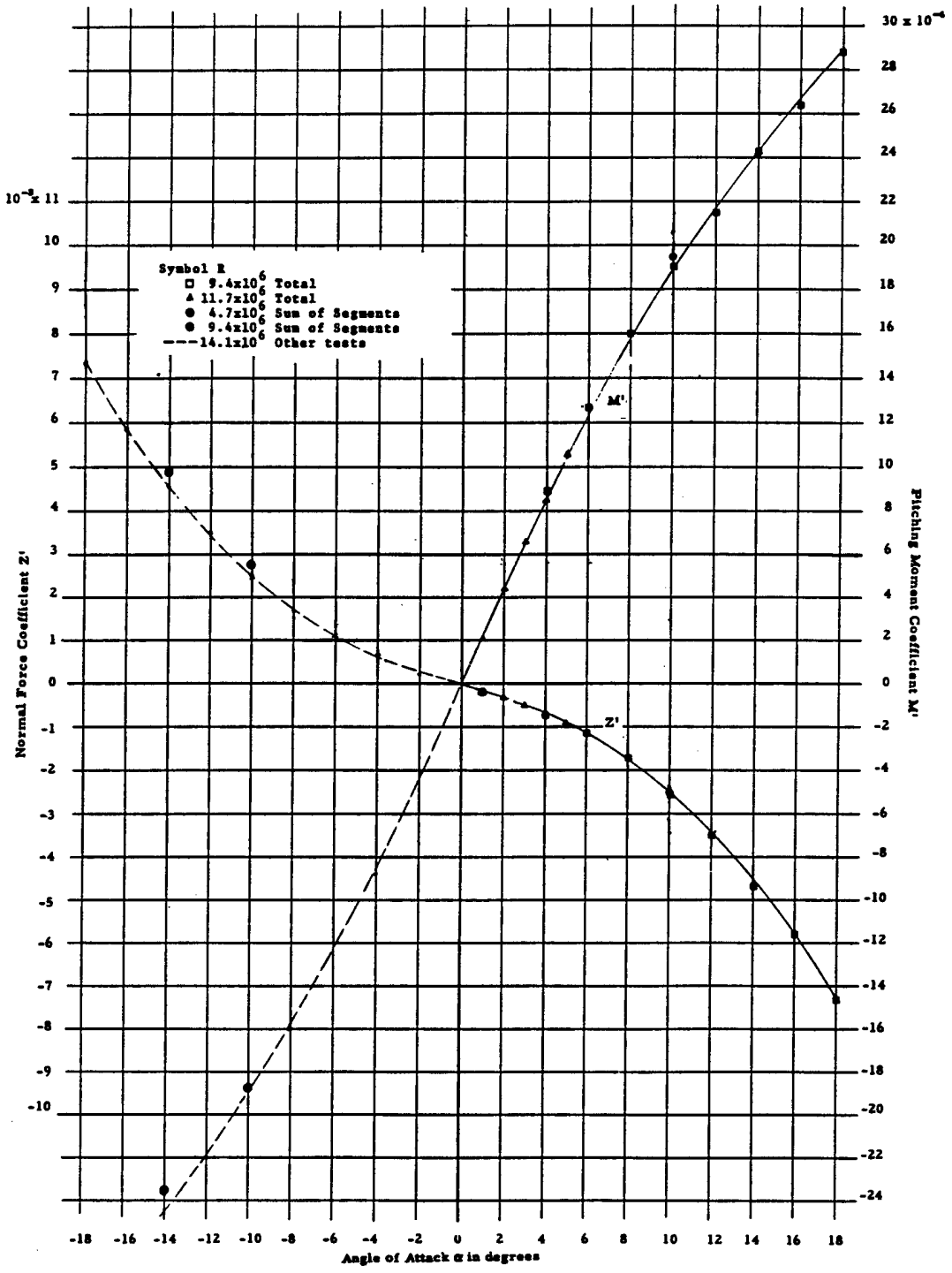

Fig. 4. Effect of angle of attack on the total normal force and pitching moment coefficients.

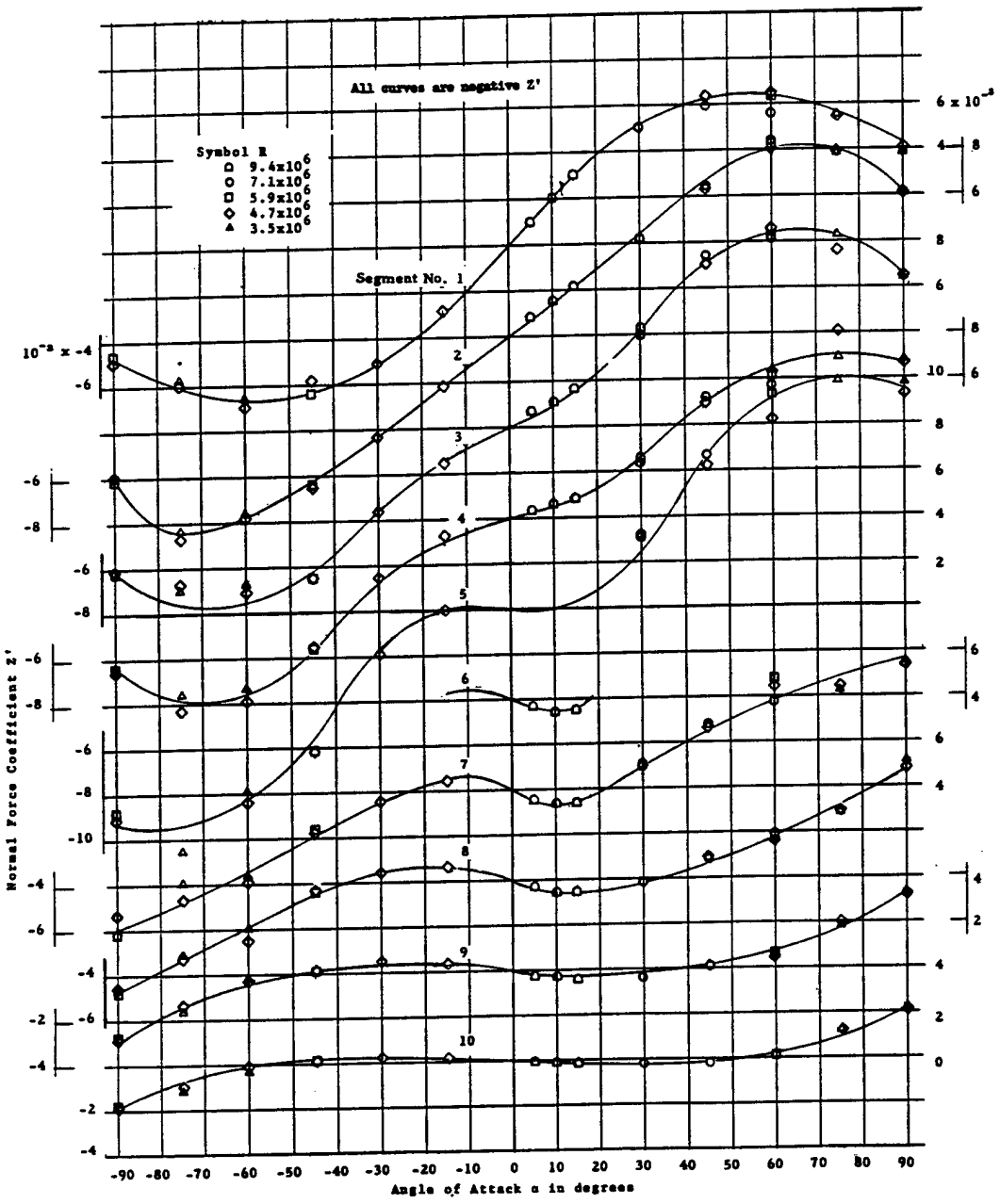

Fig. 5. Effect of large angles of attack on the normal force coefficient for each segment.

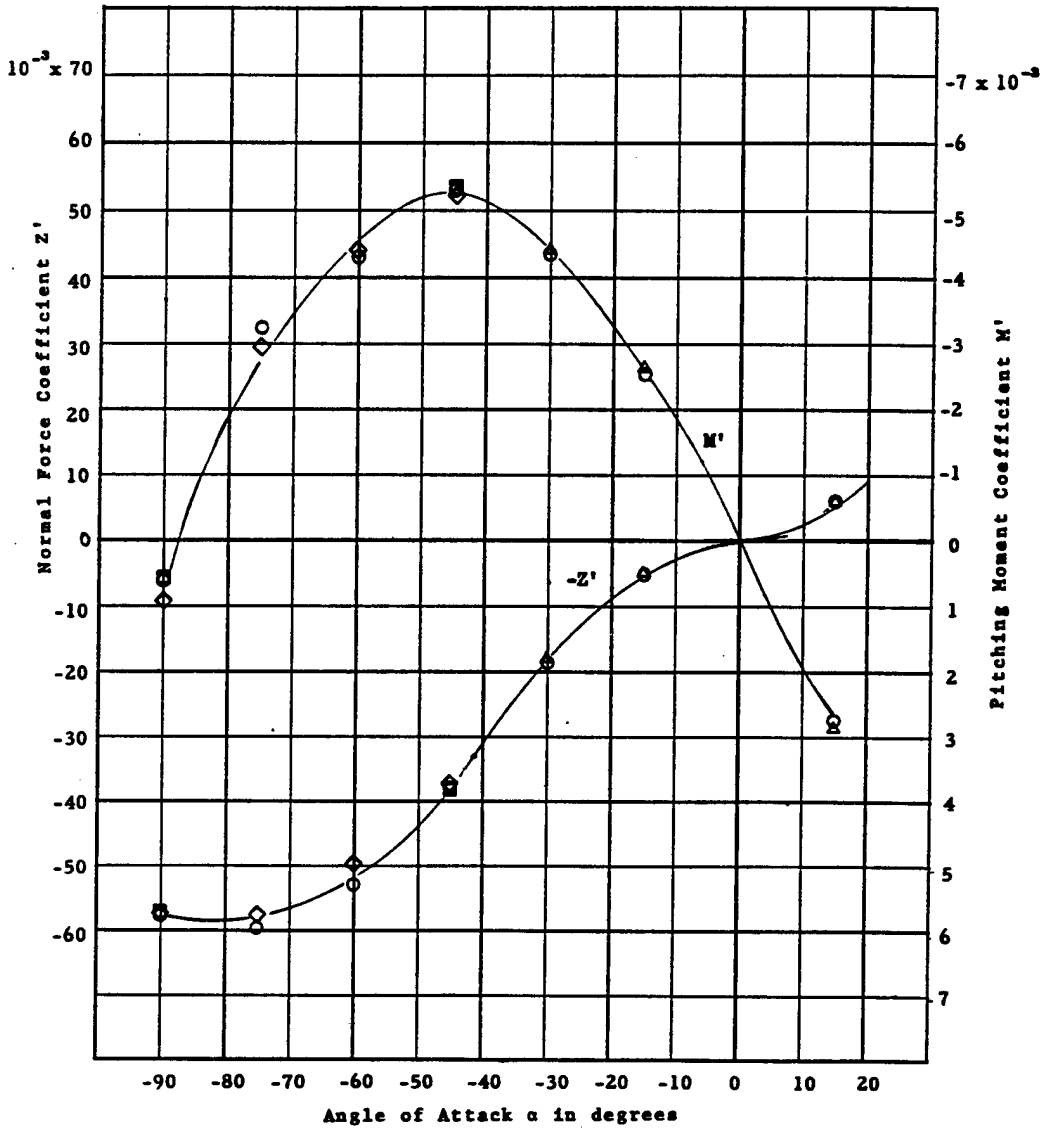

Fig. 6. Effect of large angles of attack on the normal force and pitching moment coefficients.

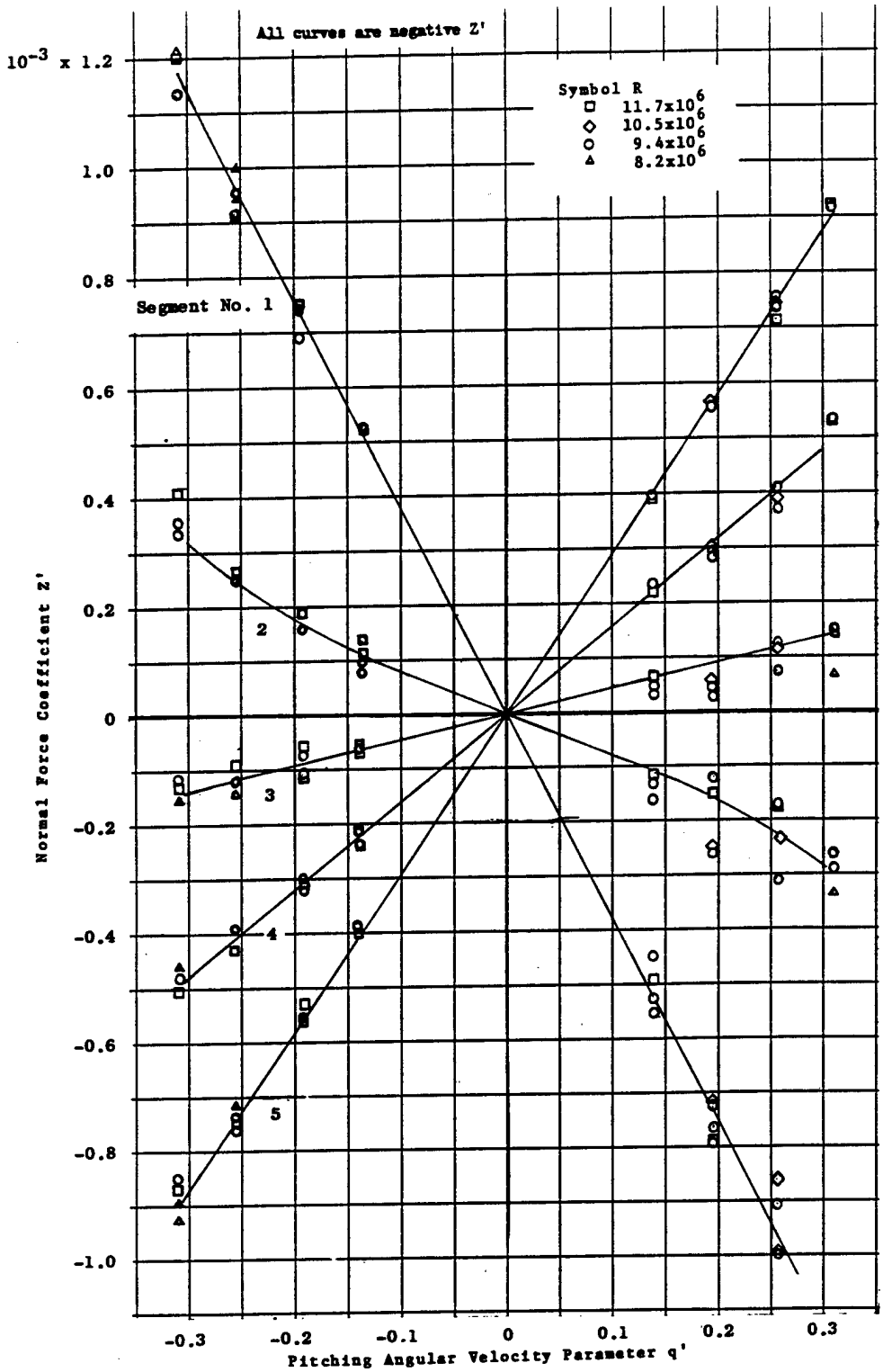

Fig. 7. Effect of pitching angular velocity parameter on the normal force coefficient for Segments 1 through 5.

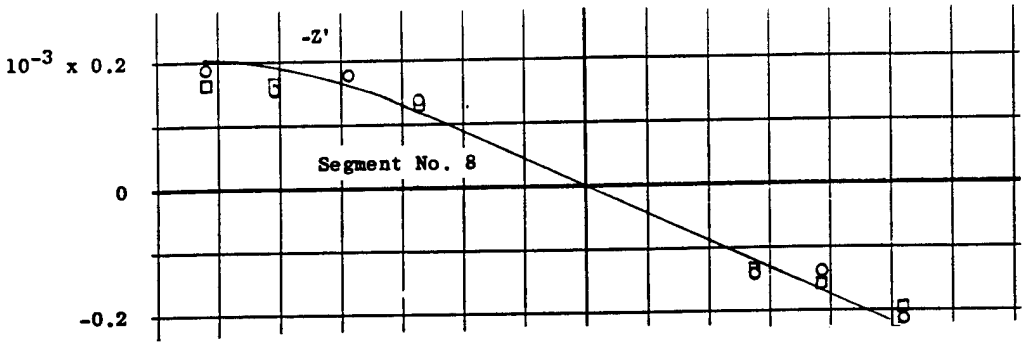

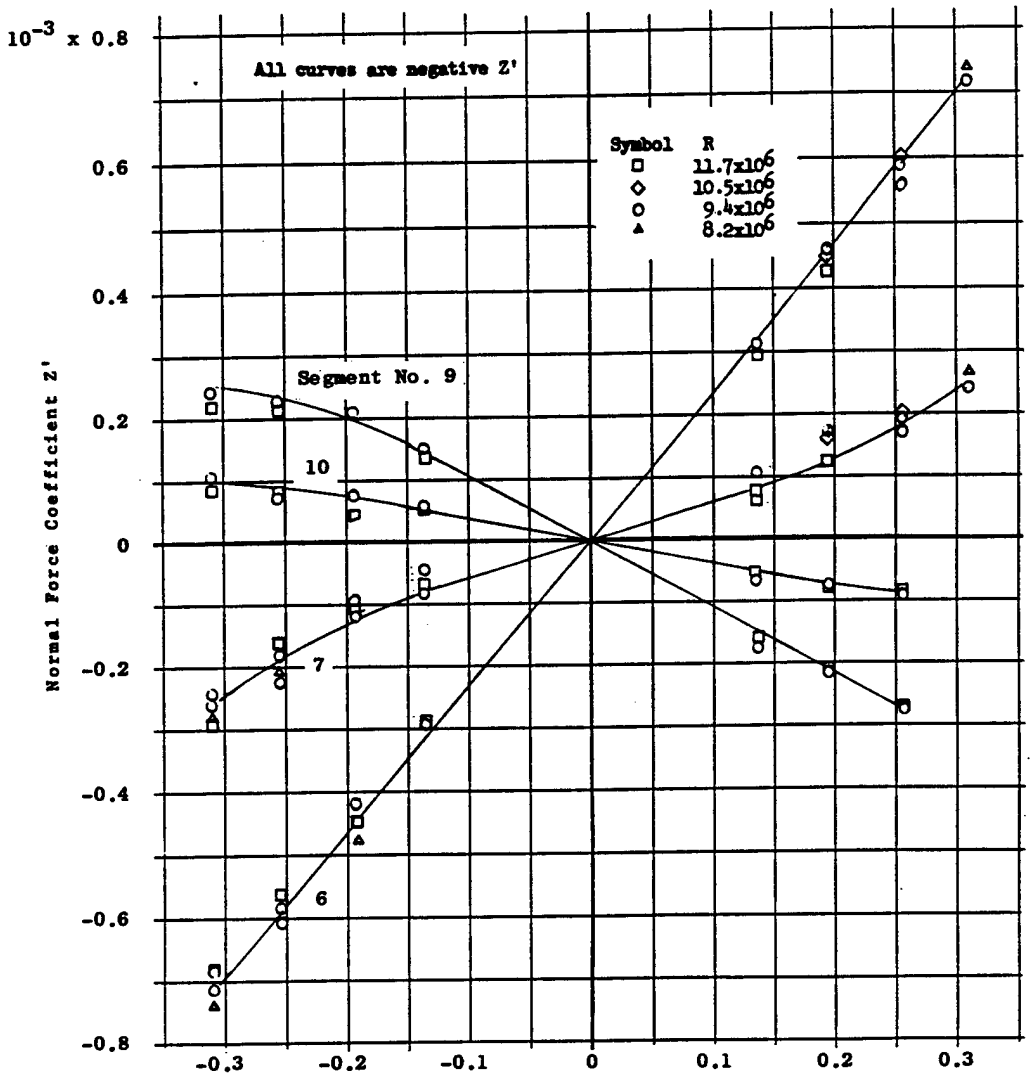

Fig. 8. Effect of pitching angular velocity parameter on the normal force coefficient for Segments 6 through 10.

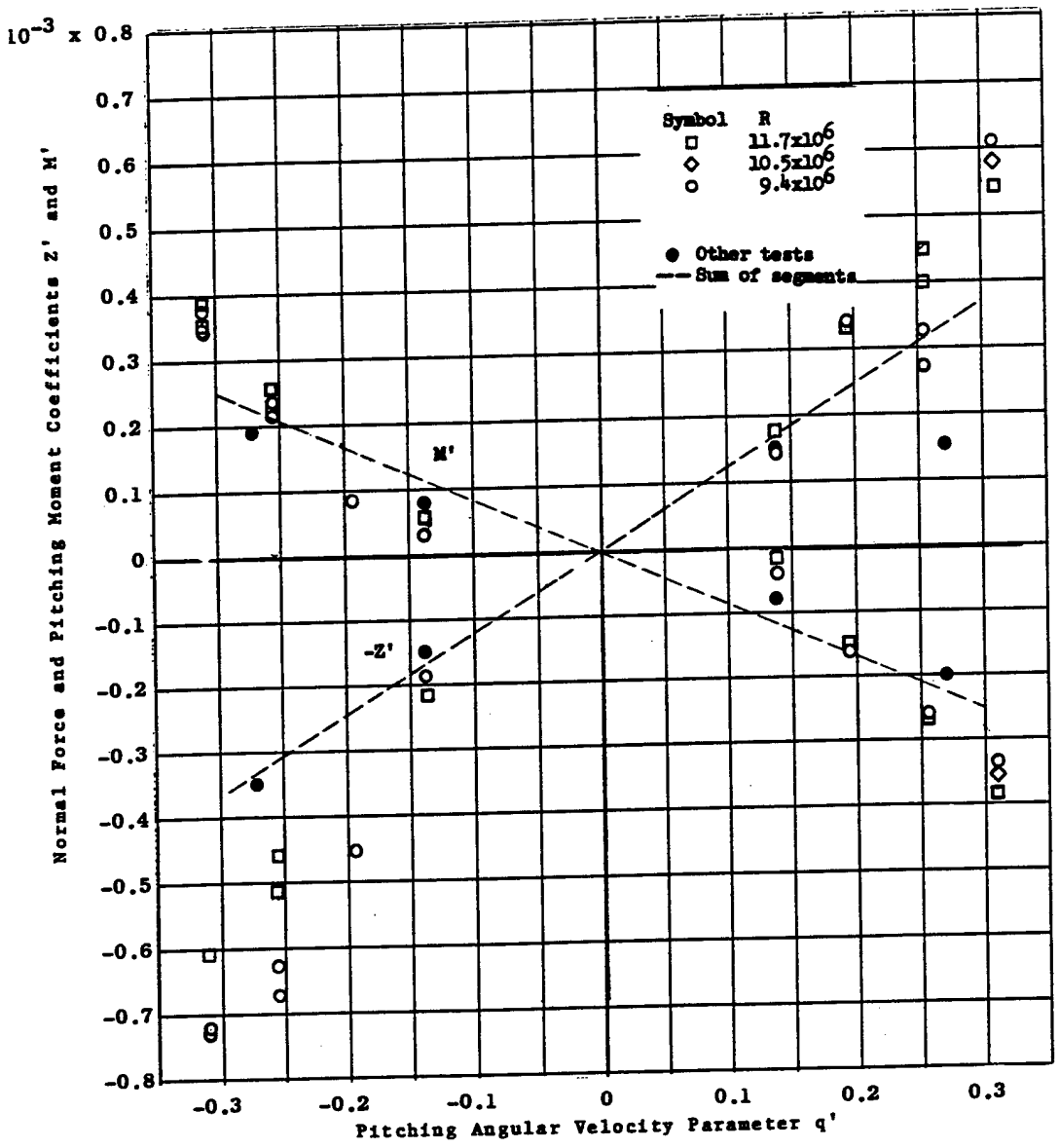

Fig. 9. Effect of pitching angular velocity parameter on the total normal force and pitching moment coefficients.

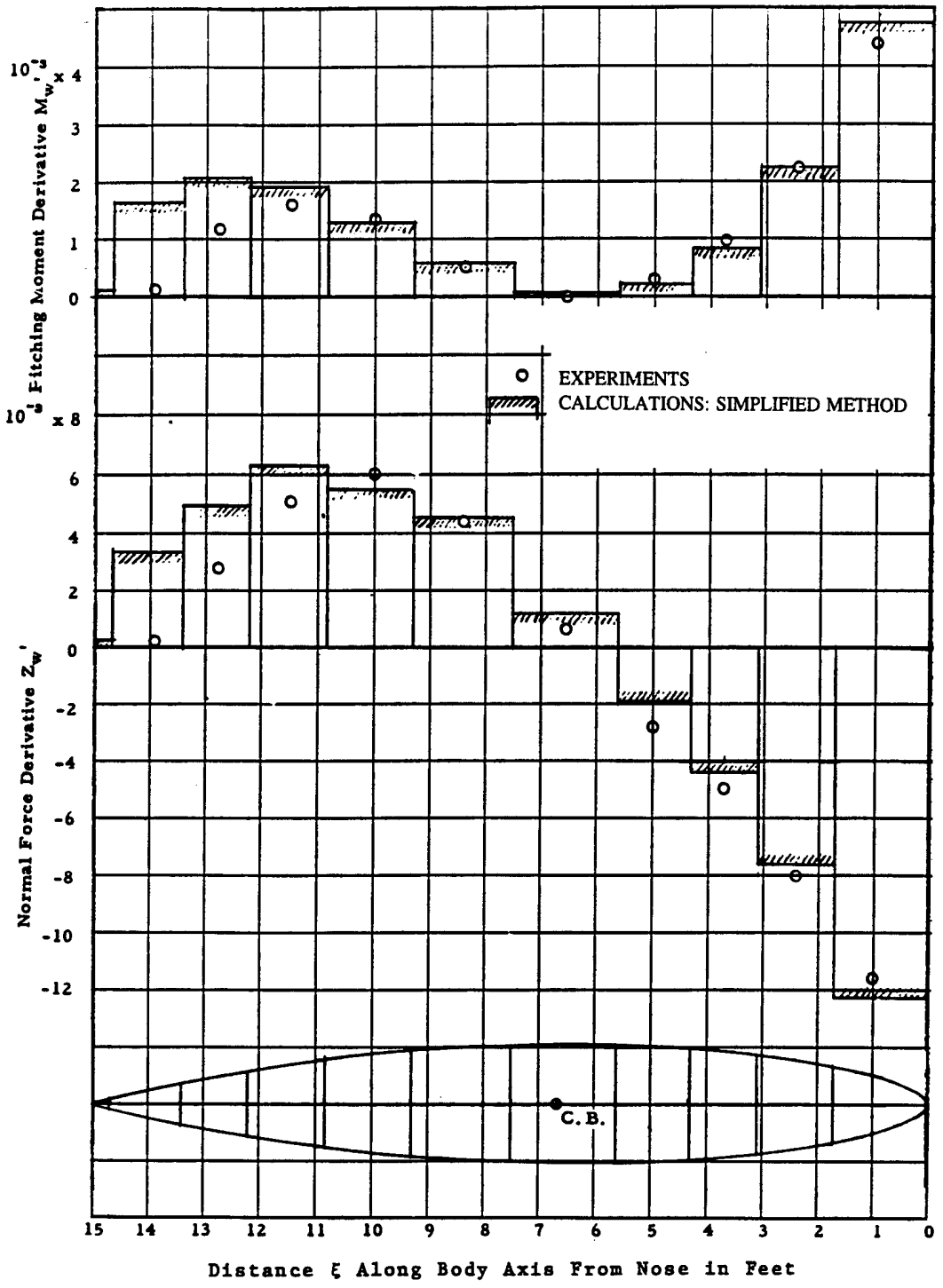

Fig. 10. Distribution of nondimensional static normal force and pitching moment derivatives along the longitudinal axis of body.

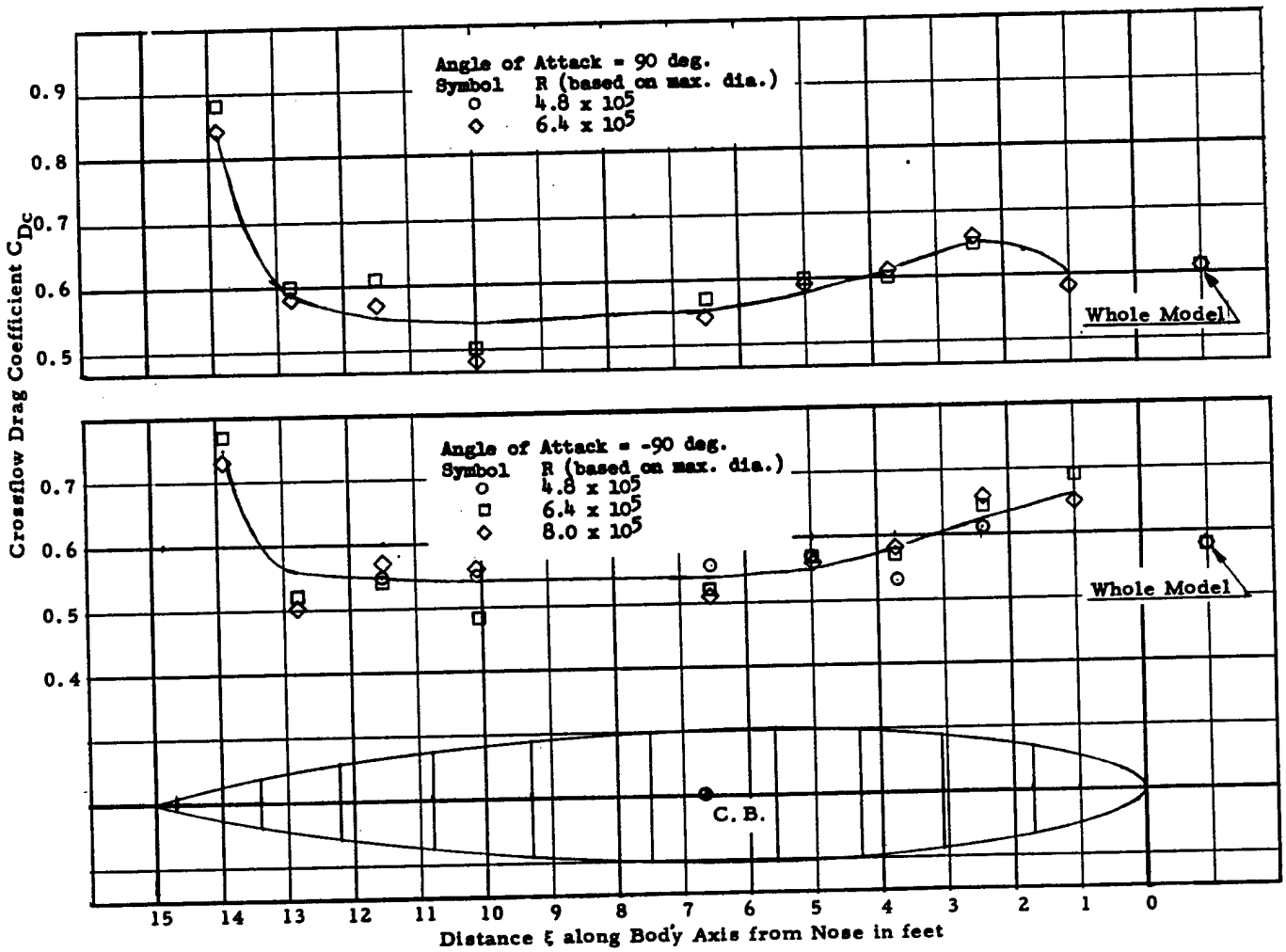

Fig. 11. Distribution of cross-flow drag coefficient along the longitudinal axis of body

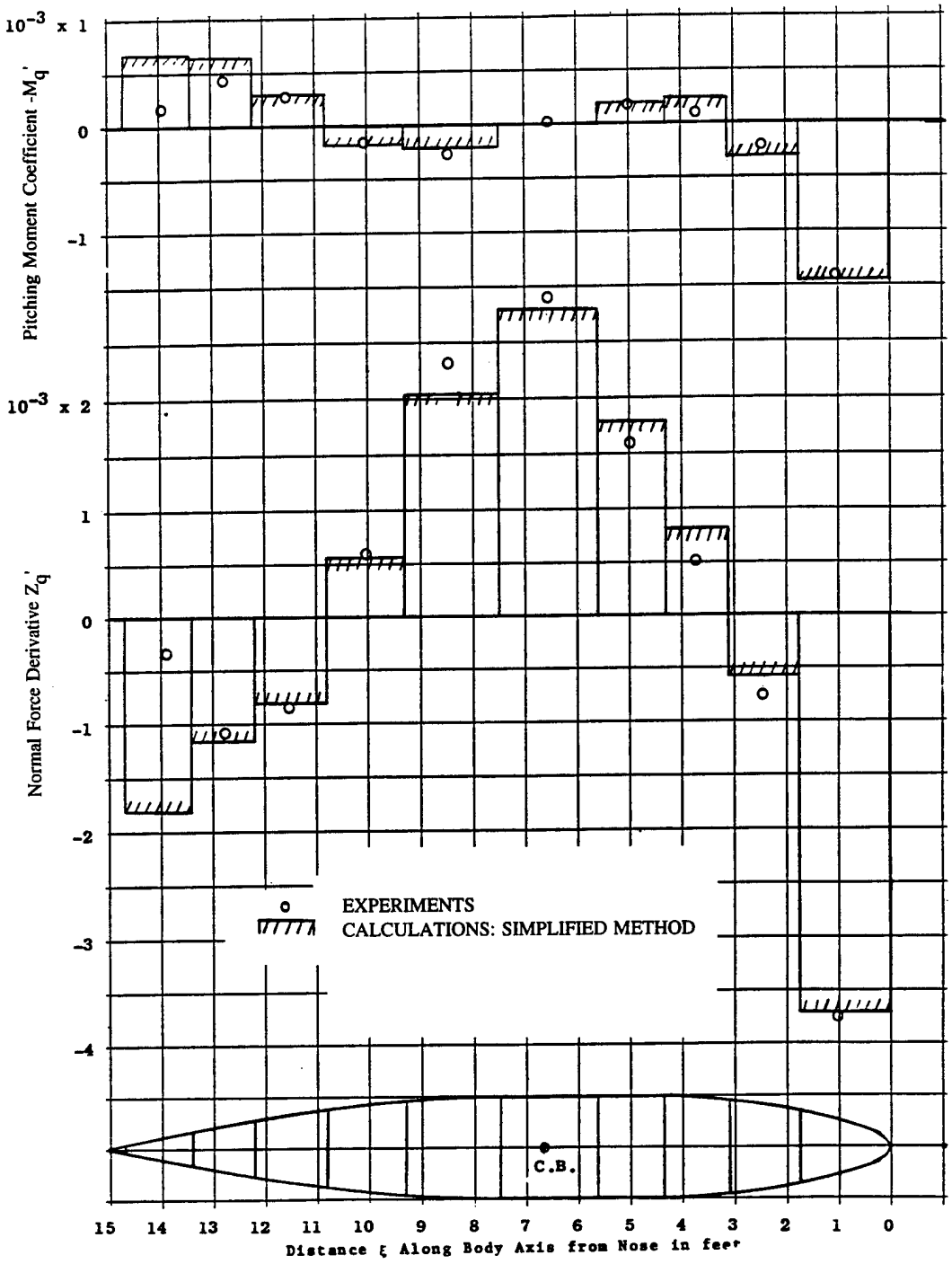

Fig. 12. Distribution of nondimensional rotary normal force and pitching moment derivatives along the longitudinal axis of body.

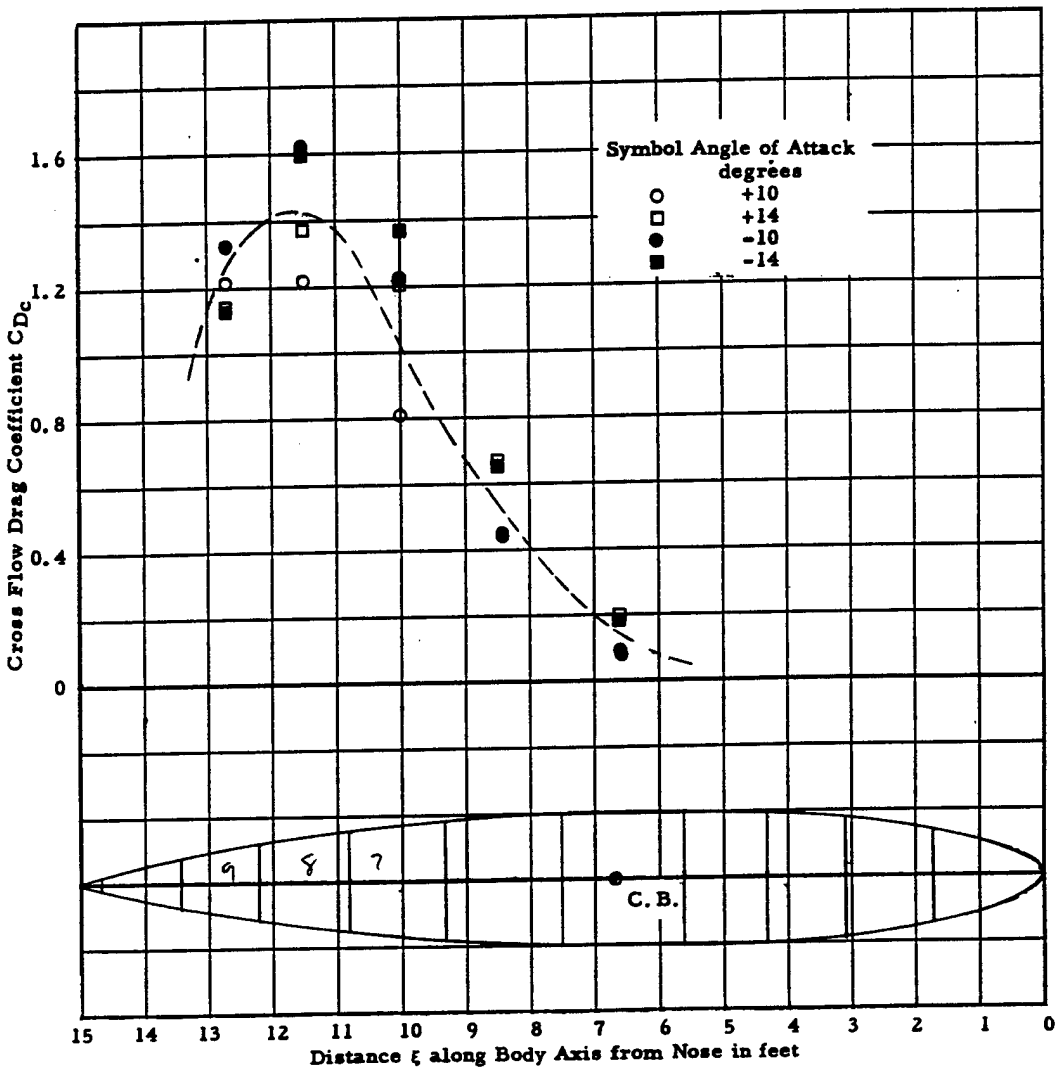

Fig. 13. Distribution of cross-flow drag coefficient along the longitudinal axis of body for angles of attack of ±10 and ±14 degrees.

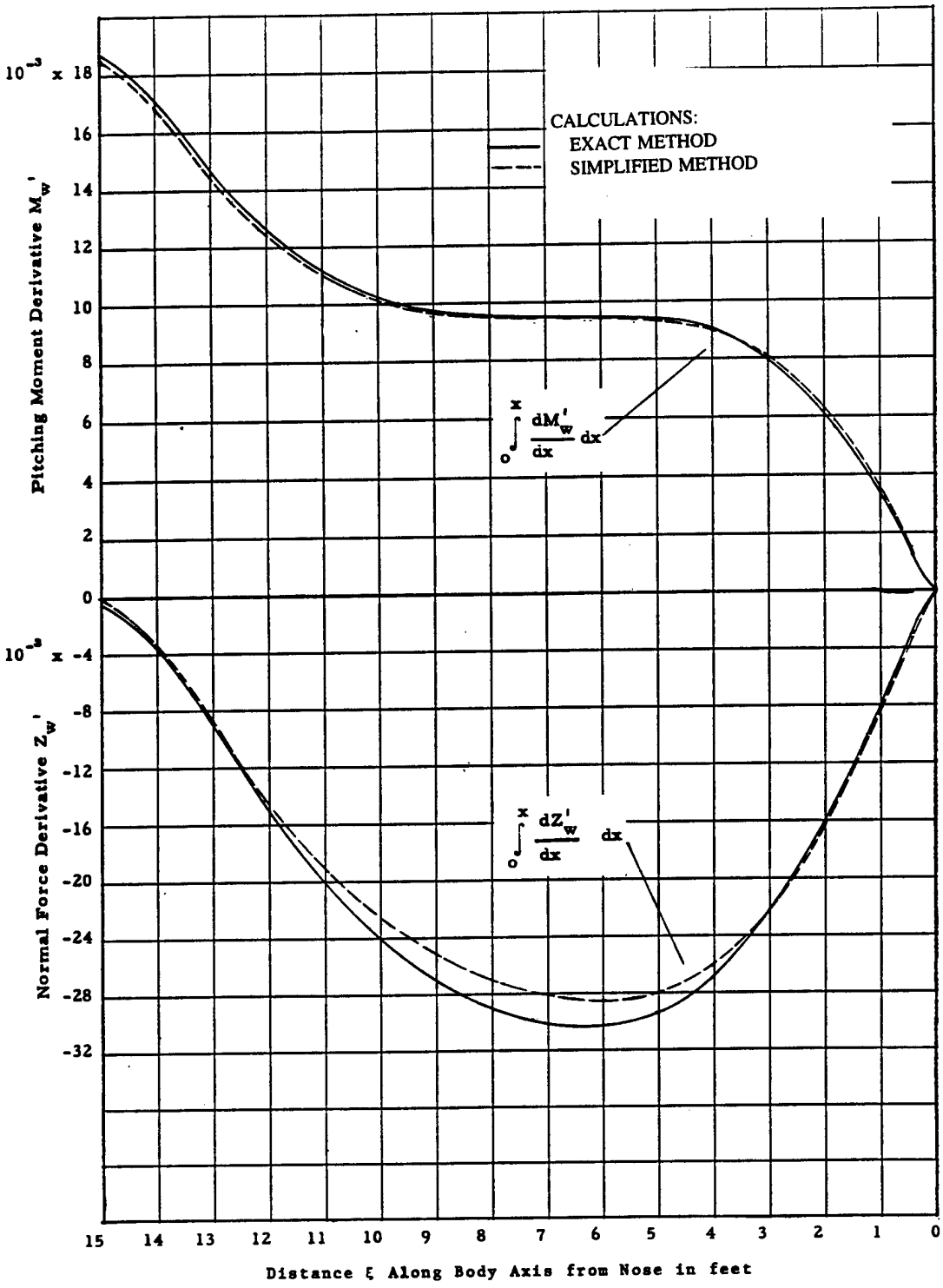

Fig. 14. Cumulative distribution of nondimensional static normal force and pitching moment derivatives along the longitudinal axis of body for Series 58 Model 4157 calculated using two analytical methods.

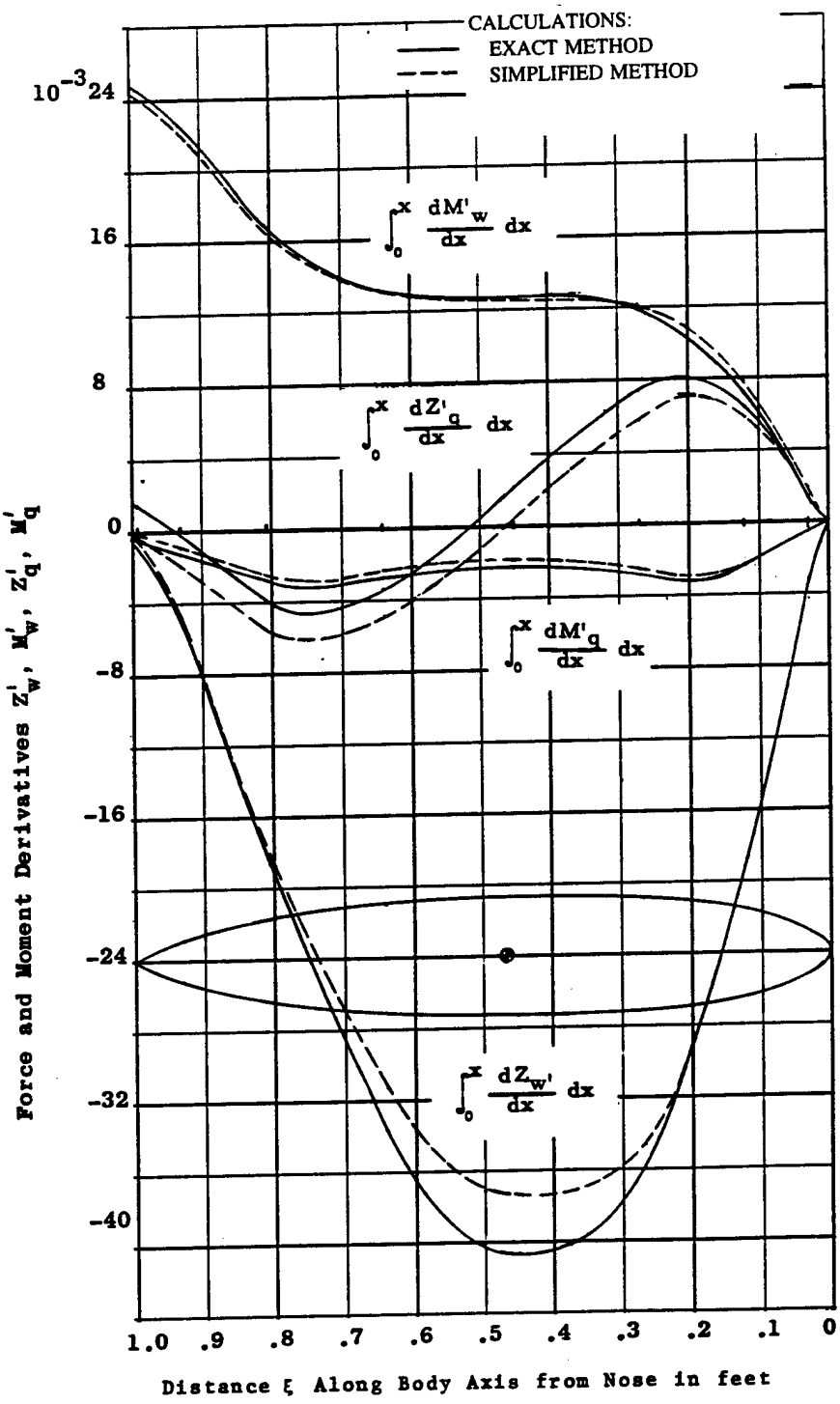

Fig. 15. Cumulative distribution of nondimensional static and rotary normal force and pitching moment derivatives along the longitudinal axis of body for Series 58 Model 4156 calculated using two analytical methods.

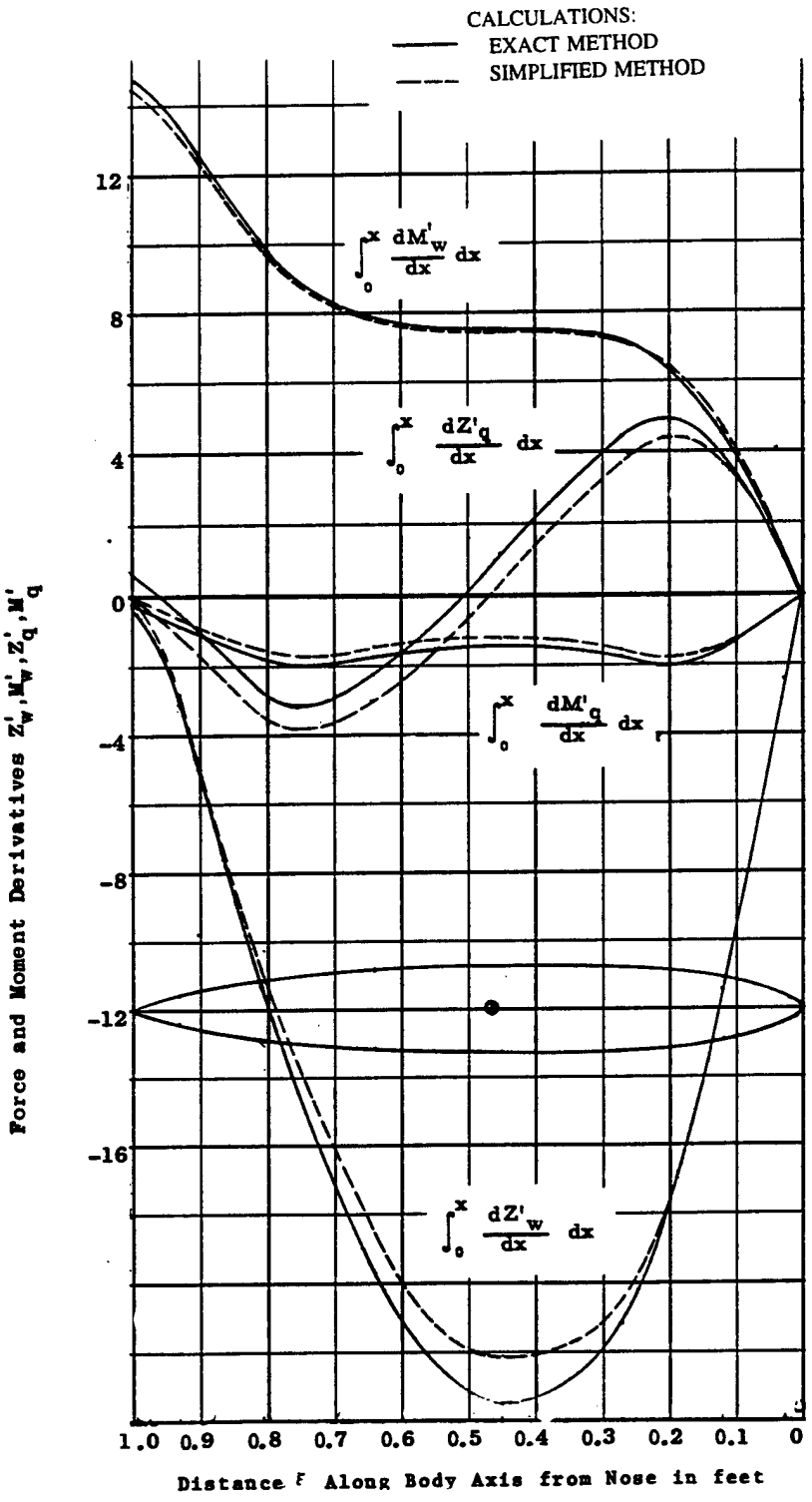

Fig. 16. Cumulative distribution of nondimensional static and rotary normal force and pitching moment derivatives along the longitudinal axis of body for Series 58 Model 4158 calculated using two analytical methods.

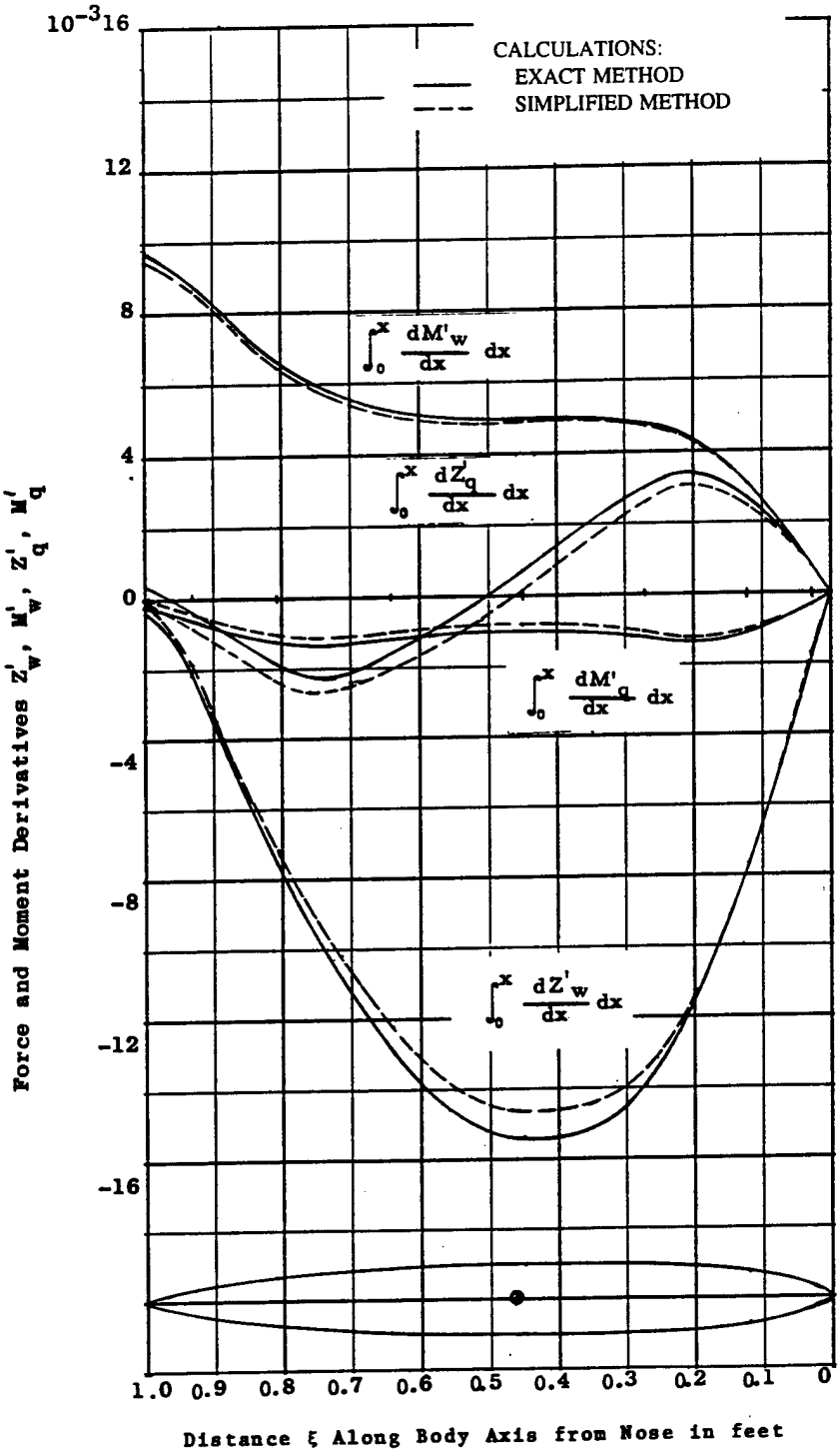

Fig. 17. Cumulative distribution of nondimensional static and rotary normal force and pitching moment derivatives along the longitudinal axis of body for Series 58 Model 4159 calculated using two analytical methods.

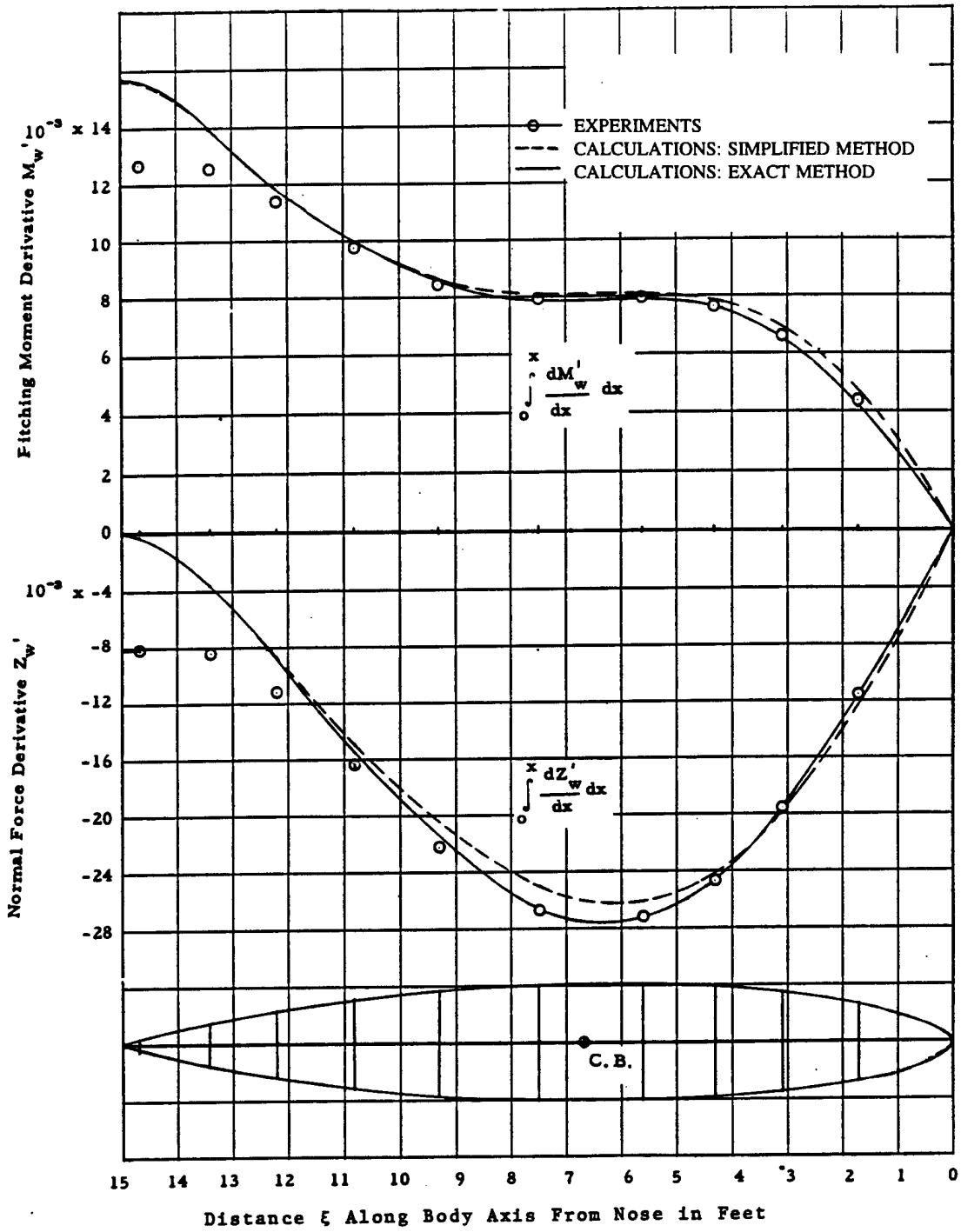

Fig. 18. Cumulative distribution of nondimensional static and rotary normal force and pitching moment derivatives along the longitudinal axis of body for Series 58 Model 4159 calculated using two analytical methods and from experimental data.

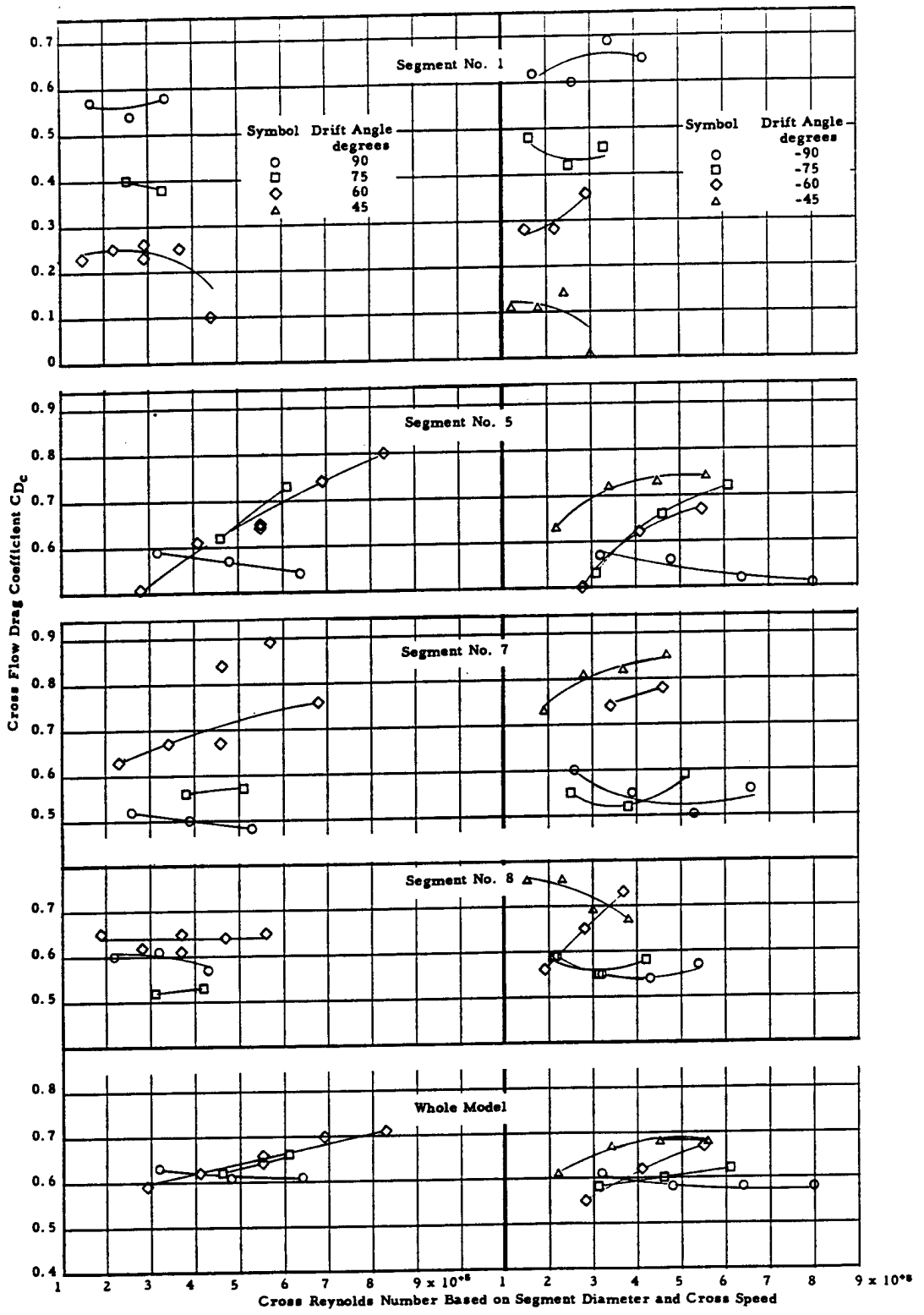

Fig. 19. Effect of cross-flow Reynolds number on cross-flow drag coefficient at various angles of attack for Segments 1, 5, 7, and 8 and for the entire body.

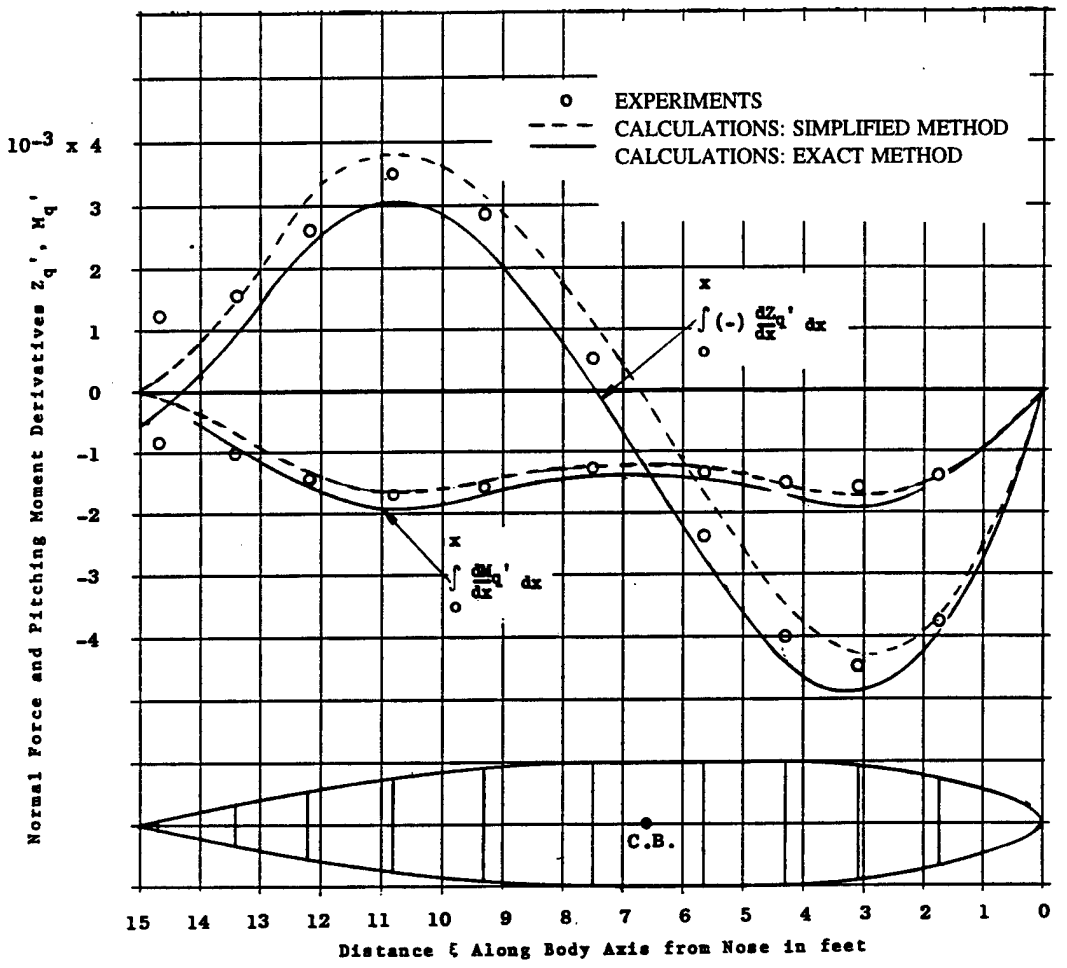

Fig. 20. Cumulative distribution of nondimensional rotary normal force and pitching moment derivatives along the longitudinal axis of body calculated using two analytical methods and from experimental data for Model 4621.

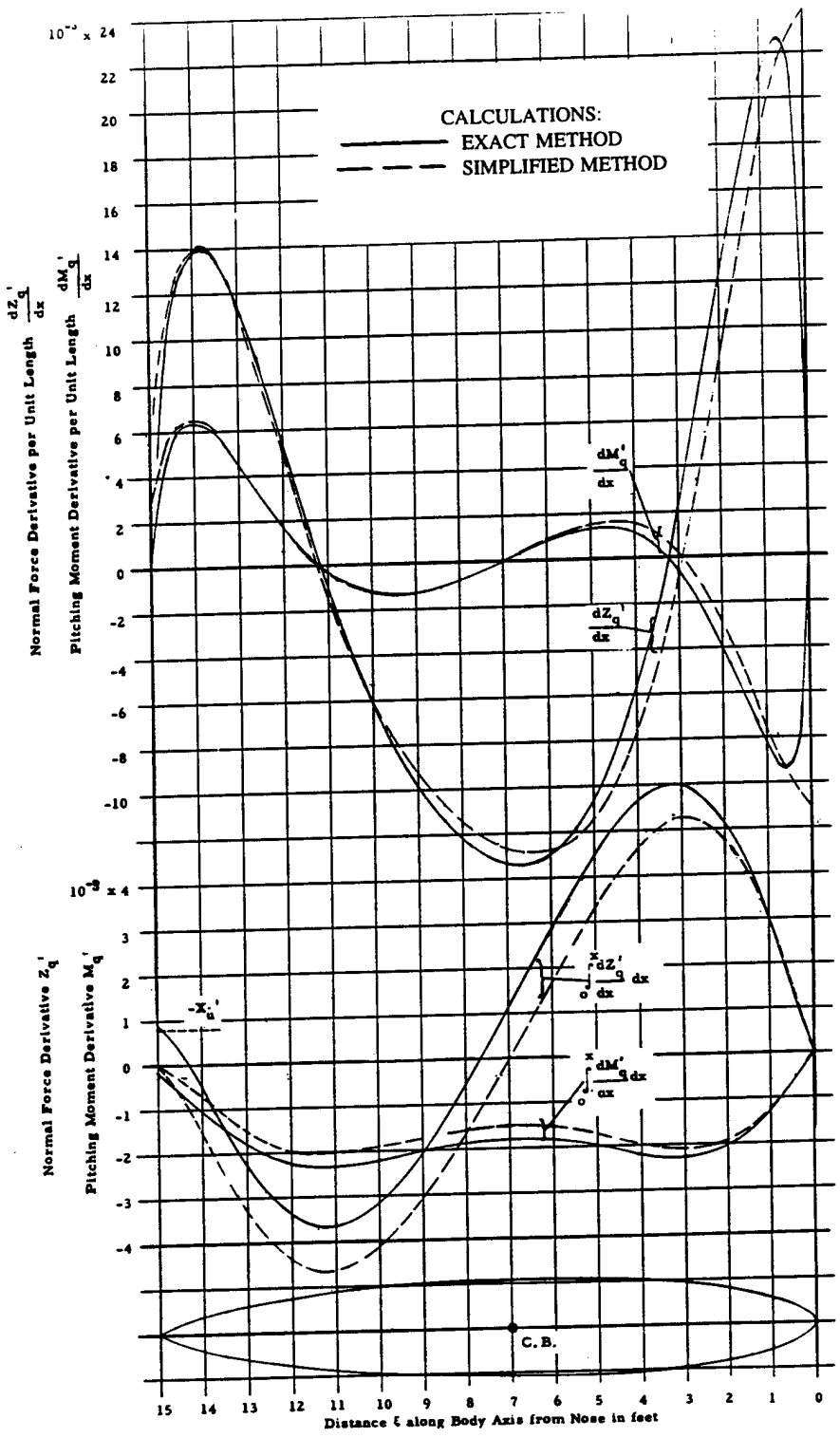

Fig. 21. Cumulative distribution of nondimensional rotary normal force and pitching moment derivatives and derivatives per unit length along the longitudinal axis of body calculated using two analytical methodsss for Series 58 Model 4157.

THIS PAGE INTENTIONALLY LEFT BLANK.

INITIAL DISTRIBUTION

Copies	Organization	Code	Name
1	ONR	333	Dr. P. Purtell
1	NAVSEA	05H2	M. King
2	DTIC		
1	NSWCCD	342	TIC(C)
1	NSWCCD	5010	Administrative Office
10	NSWCCD	5060	D. Walden
1	NSWCCD	5600	Dr. I-Y. Koh
1	NSWCCD	5600	T. Moran

THIS PAGE INTENTIONALLY LEFT BLANK.